PLANT Physiology®

Research Article

A dual role for glutathione transferase U7 in plant growth and protection from methyl viologen-induced oxidative stress

José Manuel Ugalde [ID] ,[1,2] Liliana Lamig,[2] Ariel Herrera-Vásquez [ID] ,[2,†] Philippe Fuchs [ID] ,[1]
Maria Homagk [ID] ,[1] Stanislav Kopriva [ID] ,[3] Stefanie J. Müller-Schüssele [ID] ,[1] Loreto Holuigue [ID] [2,‡] and
Andreas J. Meyer [ID] [1,*]

1   Institute of Crop Science and Resource Conservation (INRES), University of Bonn, 53113 Bonn, Germany
2   Departamento de Genética Molecular y Microbiología, Facultad de Ciencias Biológicas, Pontificia Universidad Católica de Chile, Santiago 8331150,
     Chile
3   Institute for Plant Sciences, Cluster of Excellence on Plant Sciences (CEPLAS), University of Cologne, 50674 Cologne, Germany

*Author for communication: andreas.meyer@uni-bonn.de
†Present address: Centro de Biotecnología Vegetal, Facultad de Ciencias de la Vida, Universidad Andres Bello, Santiago, Chile
‡Senior author

Abstract

Plant glutathione S-transferases (GSTs) are glutathione-dependent enzymes with versatile functions, mainly related to detoxification of electrophilic xenobiotics and peroxides. The Arabidopsis (Arabidopsis thaliana) genome codes for 53 GSTs, divided into seven subclasses; however, understanding of their precise functions is limited. A recent study showed that class II TGA transcription factors TGA2, TGA5, and TGA6 are essential for tolerance of UV-B-induced oxidative stress and that this tolerance is associated with an antioxidative function of cytosolic tau-GSTs (GSTUs). Specifically, TGA2 controls the expression of several GSTUs under UV-B light, and constitutive expression of GSTU7 in the tga256 triple mutant is sufficient to revert the UV-B-susceptible phenotype of tga256. To further study the function of GSTU7, we characterized its role in mitigation of oxidative damage caused by the herbicide methyl viologen (MV). Under non-stress conditions, gstu7 null mutants were smaller than wild-type (WT) plants and delayed in the onset of the MV-induced antioxidative response, which led to accumulation of hydrogen peroxide and diminished seedling survival. Complementation of gstu7 by constitutive expression of GSTU7 rescued these phenotypes. Furthermore, live monitoring of the glutathione redox potential in intact cells with the fluorescent probe Grx1-roGFP2 revealed that GSTU7 overexpression completely abolished the MV-induced oxidation of the cytosolic glutathione buffer compared with WT plants. GSTU7 acted as a glutathione peroxidase able to complement the lack of peroxidase-type GSTs in yeast. Together, these findings show that GSTU7 is crucial in the antioxidative response by limiting oxidative damage and thus contributes to oxidative stress resistance in the cell.

Open Access

Introduction

In plants, animals, and prokaryotes, glutathione S-transferases (GSTs) constitute a large family of enzymes with a wide range of cellular functions (Basantani and Srivastava, 2007). In plants, GSTs are mainly involved in the detoxification of exogenous xenobiotics and intracellular oxidized molecules, such as lipid peroxides, to alleviate chemical and oxidative damage (Sappl et al., 2009; Chronopoulou et al., 2017a) and anthocyanin transport to the vacuole (Alfenito et al., 1998; Mueller et al., 2000; Gomez et al., 2011). GST-mediated cellular detoxification is largely based on two enzymatic activities: the transferase and the peroxidase activities. As transferases, GSTs mediate the conjugation of the reduced tripeptide glutathione (GSH) with the electrophilic center of different organic molecules (Dixon and Edwards, 2010; Labrou et al., 2015). The resulting conjugates are subsequently exported from the cytosol to the vacuole or the apoplast (Cummins et al., 2011). As peroxidases, some GSTs exhibit a GSH-dependent glutathione peroxidase (GPOX) activity which allows the reduction of lipid peroxides to alcohols (Edwards et al., 2000; Dixon et al., 2009). Plant GSTs are also involved in other processes such as secondary metabolism and development (Roxas et al., 1997; Chen et al., 2007; Dixon et al., 2010). Expression of several GSTs is boosted under biotic and abiotic stresses, for example pathogen infection (Mauch and Dudler, 1993), high salt concentrations (Roxas et al., 2000; Du et al., 2019), hypoxia (Moons, 2003), UV-B radiation (Loyall et al., 2000), exposure to safeners (DeRidder et al., 2002; Cummins et al., 2009), herbicides (Dixon and Edwards, 2010), oxylipins (Mueller et al., 2008; Stotz et al., 2013), or salicylic acid (SA) (Chen et al., 1996; Sappl et al., 2009). The common denominator of these stress conditions is that they all trigger the production of reactive oxygen species (ROS) and hence cause oxidative stress. The induction of GSTs across this extensive span of conditions and treatments has strongly reinforced the idea of their protective role against oxidative stress (Chen et al., 2012; Chronopoulou et al., 2017b).

In Arabidopsis (Arabidopsis thaliana), the GST gene family counts 53 members of which only a few are functionally characterized (Sylvestre-Gonon et al., 2019). Based on their protein sequence and function, the GSTs are divided into seven distinct subclasses (Supplemental Figure S1, A; Wagner et al., 2002). The subclasses phi (F) and tau (U) are plant-specific and constitute the largest classes with 14 and 28 members, respectively (Chronopoulou et al., 2017a). Tolerance to herbicides mediated by GSTs relies on the capacity of GSTUs and GSTFs to conjugate electrophilic herbicides or their derivatives to GSH (Cummins et al., 1999; Edwards et al., 2000). Furthermore, studies on weeds indicate that herbicide resistance is mediated by GSTF isoforms and depends on preventing the accumulation of cytotoxic organic hydroperoxides caused by herbicide applications, rather than by the direct detoxification of the herbicide itself (Cummins et al., 1999).

The detoxification activities of GSTs strictly depend on GSH and thus are tightly interconnected with the cellular redox state (Dixon and Edwards, 2010). GSH is the most abundant low-molecular-weight thiol in the cell and is involved in a number of key cellular functions. Direct or indirect use of GSH as an electron donor for ROS scavenging leads to formation of glutathione disulfide (GSSG) (Noctor et al., 2012). Based on in vivo measurements with genetically encoded fluorescent probes, the GSH/GSSG ratio in subcellular compartments that contain a functional glutathione reductase has been calculated to be in the order of 50,000:1 (Schwarzländer et al., 2016). Stress situations and experimental systems like treatment with bacterial elicitors cause a pronounced oxidative shift (Nietzel et al., 2019). The shift in the GSH/GSSG ratio is a key feature of stress responses and is considered to be important for downstream signaling pathways and developmental programs (Meyer, 2008).

Methyl viologen (MV) is a broad-spectrum herbicide that acts in chloroplasts by redirecting electrons originating from photosystem I (PSI) to molecular oxygen (O_2), which generates superoxide ($O_2^{\cdot-}$) (Mano et al., 2001; Scarpeci et al., 2008). The enhanced production of $O_2^{\cdot-}$ has made MV a model for photooxidative stress in plants and it has been shown recently that MV-induced photooxidative stress in plastids causes a pronounced release of H_2O_2 into the cytosol (Ugalde et al., 2021). Similarly, in non-photosynthetic organisms, MV redirects electrons from complex I of the mitochondrial electron transport chain to O_2, which also generates $O_2^{\cdot-}$ (Cochemé and Murphy, 2008). Increased ROS production leads to lipid peroxidation, which is considered to be the main cause of MV toxicity in plant and mammalian cells (Bus et al., 1976; Misra and Gorsky, 1981; Liu et al., 2009).

Studies in plants have already demonstrated that GSTs contribute to MV tolerance. For instance, heterologous overexpression of cotton GST-cr1 in tobacco (Nicotiana tabacum) (Yu et al., 2003), a Suaeda salsa GST in rice (Zhao and Zhang, 2006), and rice GSTU4 in Arabidopsis (Sharma et al., 2014), as well as homologous overexpression of GSTU51 in poplar (Choi et al., 2013) and GSTU19 in Arabidopsis (Xu et al., 2016), consistently led to an improved MV tolerance when compared with wild-type (WT) controls. All these studies established a link between the tolerance phenotype and either an increased enzymatic antioxidant activity (GPOX, GST, CAT) and reduced oxidative damage upon MV treatment. The molecular function of GSTs in this context, however, remains unknown.

Expression of GSTU7 has been reported to be induced in plants exposed to a wide range of stress stimuli including the exposure to heavy metals (Becher et al., 2004), to oxylipins and phytoprostanes (Loeffler et al., 2005; Mueller et al., 2008; Stotz et al., 2013) and to SA (Blanco et al., 2009). SA also promotes the accumulation of GSTU7 protein in cell cultures (Sappl et al., 2004; Gruhler et al., 2005). For oxylipin treatment, expression of GSTU7 has been shown to be controlled by class II TGA transcription factors (TGA2, 5, and 6)

(Stotz et al., 2013). Independent findings further support a role of class II TGA transcription factors in controlling the expression of a group of genes with putative antioxidant functions in response to SA (Blanco et al., 2009) and UV-B stress (Herrera-Vásquez et al., 2021). In the latter work, *tga2 tga5 tga6* triple mutants (*tga256*) were more susceptible to oxidative stress caused by UV-B similar to the susceptibility of *tga256* to SA established earlier (Zhang et al., 2003). Interestingly, at least 12 GSTUs including GSTU7 were induced by UV-B and shown to be controlled by the class II TGA transcription factors. The role of TGAs in expression of GSTU7 was further confirmed in ChIP assays showing binding of TGA2 to the palindromic TGA-box (TGACGTCA) in the *GSTU7* promoter region under stress conditions in vivo (Herrera-Vásquez et al., 2021). It is unclear though why GSTU7 would be beneficial in stress situations that activate class II TGAs.

The large number of GSTs in plants and widespread functional redundancy among them make it challenging to study the function of specific GSTs and, therefore, little is known about their individual roles in Arabidopsis. In this study, we report a role of GSTU7 in plant growth and characterize GSTU7 as a key enzyme mediating the tolerance of Arabidopsis to oxidative stress induced by MV and explore its importance in cellular redox homeostasis.

Results

Expression of *GSTU7* is induced under different stress conditions

To determine regulation of *GSTU7* expression induced by different stress conditions, Arabidopsis WT seedlings were treated with either 0.5 mM SA, UV-B radiation, or 50 µM MV and *GSTU7* transcript levels determined at different time points (Figure 1, A–C). SA caused a six-fold induction of *GSTU7* expression within 30 min, leading to a peak of seven-fold transcript level after 2 h compared with non-treated controls (Figure 1, A). Between 8 and 24 h after the start of the SA incubation, *GSTU7* expression was again close to expression in control plants. UV-B radiation (Figure 1, B) induced a 2.3-fold increase in transcript levels after 2.5 h which slightly increased to three-fold at 24 h. Treatment of plants with MV resulted in the most pronounced induction of *GSTU7* expression among the three treatments with a maximum of 25-fold after 24 h (Figure 1, C).

Recently, UV-B-induced expression of 12 GSTs including *GSTU7* was found to be controlled by the class II TGA transcription factors TGA2, TGA5, and TGA6 (Herrera-Vásquez et al., 2021). To test whether the induction of *GSTU7* in response to UV-B and MV (Figure 1, B and C) is dependent on class II TGAs or SA, UV-B- and MV-induced changes in *GSTU7* transcript levels were compared between WT, the *tga256* triple mutant, and the SA-deficient mutant *sid2-2*. In contrast to the response in WT plants, induction of *GSTU7* expression was completely abolished in the *tga256* triple mutant (Figure 1, D and E). In *sid2-2* mutant, however, *GSTU7* was still induced by treatments with UV-B and MV,
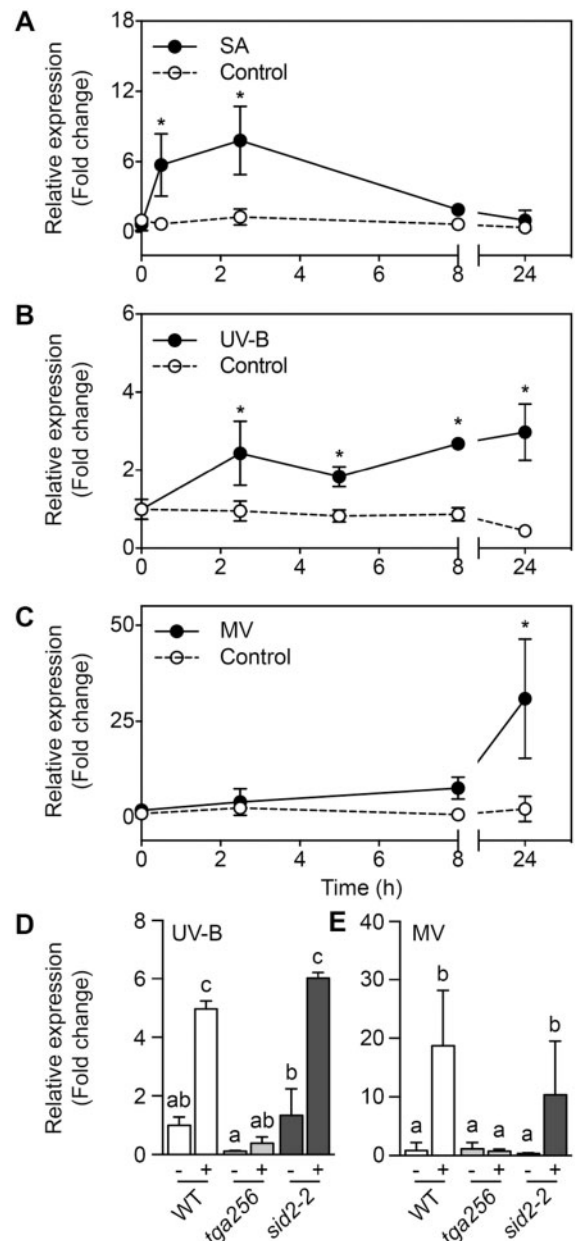

Figure 1 GSTU7 gene expression is induced by SA, UV-B radiation (UV-B), and MV. A–C, mRNA accumulation of *GSTU7* was determined by RT-qPCR in 2-week-old WT Arabidopsis seedlings treated with 0.5 mM SA in MS medium (A), UV-B radiation (B), or 50 µM MV in MS medium (C) (all shown by filled circles). For control treatments, seedlings were floated on MS medium (open circles) (A, C) or irradiated through a filter blocking UV-B (B). D and E, *GSTU7* transcript levels measured by RT-qPCR in WT, *tga256*, and *sid2-2* seedlings after 5 h of UV-B radiation (D) or after 24 h of incubation with 50 µM MV (E). Gene expression is expressed as fold change relative to a subunit of *CLATHRIN ADAPTOR COMPLEX* gene (for SA and MV) or the *YLS8* (for UV-B) housekeeping genes and normalized to the expression at 0 h (A–C) or to the expression in untreated WT seedlings (D and E). Means ± SD (A–E) were calculated from three independent biological replicates (two to three seedlings pooled per replicate). The obtained data were tested for significant differences by ANOVA with Fisher's LSD test. * indicates differences compared with the expression at the start of the treatment (0 h; $P < 0.05$). Different letters indicate statistically different groups ($P < 0.05$).

similarly to induction in WT plants (Figure 1, D and E). Altogether, the experiments showed that UV-B and MV stress-induced expression of GSTU7 is controlled by class II TGAs but not through a SA-dependent pathway.

Deletion of GSTU7 causes growth retardation

To further characterize the role of GSTU7, an insertional mutant, gstu7, was isolated and the T-DNA confirmed by sequencing to be inserted between A and T of the ATG start codon (Figure 2, A). Absence of detectable transcript confirmed gstu7 as a null mutant (Figure 2, B). For complementation, a UBQ10$_{pro}$:GSTU7-V5 construct was cloned and transformed into gstu7 plants. Two independent lines, gstu7/GSTU7-V5 #2 and gstu7/GSTU7-V5 #5, were selected from a larger pool of 16 transformants based on high expression levels and protein abundance. As expected, treatment of WT plants with 50 μM MV caused increased GSTU7 expression, while in both complemented lines, GSTU7 transcripts were detected at higher levels than in the WT, without pronounced changes after MV treatment (Figure 2, B). Constitutive expression of GSTU7-V5 was confirmed by immunodetection of the V5 tag in both lines, albeit with much higher protein abundance in line #2 than in line #5 (Figure 2, C).

Homozygous gstu7 mutants developed a dwarf phenotype with shorter roots compared with WT seedlings (Figure 2, D and E), smaller rosettes (Figure 2, F), and delayed bolting (Figure 2, G). Complementing the mutant with GSTU7-V5 restored gstu7 to a WT phenotype at all analyzed developmental stages. To confirm that the smaller phenotype of gstu7 was due to a single T-DNA insertion, gstu7 was backcrossed to a WT plant. The F2 progeny of this cross segregated with a 3:1 ratio for WT:short root mutant phenotypes ($\chi^2 = 0.067$; $P = 0.79$) (Figure 2, E).

GSTU7 mitigates oxidative stress induced by MV and 3-aminotriazole

The main function of GSTs is the detoxification of exogenously applied xenobiotics and endogenously generated organic peroxides, such as lipid peroxides (Sappl et al., 2009; Chronopoulou et al., 2017a). To further test whether GSTU7 is involved in developing plant tolerance to oxidative stress, the effect of MV on growth of WT, gstu7, and the two complemented lines #2 and #5 was investigated (Figure 3, A). Seedling tolerance to 0.1 μM MV was determined as survival rates after germination on plates containing MV and documented as the percentage of seedlings with green tissue relative to the total number of germinated seedlings following established protocols (Laporte et al., 2012). gstu7 showed a survival rate of 29% compared with WT seedlings of which 62% survived (Figure 3, A). Constitutive overexpression of GSTU7 cured the apparent increased susceptibility of gstu7 toward MV and led to a survival rate of about 90%, which is significantly higher than in WT plants ($P = 0.0003$). The same general pattern with increased sensitivity in gstu7 and diminished sensitivity in complemented gstu7 lines was found when seedlings were transferred to plates containing

50 nM MV after germination and then grown for 17 d (Figure 3, B).

The role of GSTU7 for alleviating herbicide-induced oxidative stress was also tested upon treatments with the catalase inhibitor 3-aminotriazole (3-AT), which is known to induce oxidative stress (May and Leaver, 1993; Figure 3, B and C). After germination on MS medium, WT, gstu7, and the complemented lines were transferred either to plates with MS or MS supplemented with 1 μM 3-AT (Figure 3, B). Herbicide tolerance was quantified for each line as the relative growth compared with the respective controls grown on MS without 3-AT. For WT seedlings, 3-AT restricted the growth to 74% compared with non-treated controls. This growth restriction was far more pronounced in gstu7, which reached only 30% of the biomass of the respective control seedlings grown without 3-AT (Figure 3, C). Both complemented lines on average reached 52% and 62% of the biomass of seedlings not treated with 3-AT and thus performed better than gstu7 on 3-AT.

Unlike the distinct sensitivity of gstu7 toward MV and 3-AT, the mutant did not show increased susceptibility toward pathogen infection with Pseudomonas syringae DC3000 AvrRpt2. While mutant lines, such as sid2-2 and tga256, which are known to be more susceptible (Zhang et al., 2003; Seguel et al., 2018), showed severe cell damage and ion leakage after infection and thus a high relative conductivity in the medium, the susceptibility of gstu7 mutants and the respective complementation lines were very similar to the WT plants (Supplemental Figure S2).

To further assess whether the increased susceptibility of gstu7 mutants to MV corresponds with a higher production of ROS, primary leaves were treated with a 2 μL drop of 30 μM MV, incubated under constant light conditions for 24 h and subsequently stained with 3,3′-diaminobenzidine (DAB) for hydrogen peroxide (H_2O_2) detection (Figure 3, D). For assessment of the staining, the DAB-stained areas on each leaf were masked out and set into relation to the whole area of the respective leaf (Figure 3, D). After MV treatment, gstu7 seedlings had a three-fold larger area of intense staining than WT seedlings, which indicates the presence of increased amounts of H_2O_2. In contrast, complemented gstu7 seedlings after MV treatment showed even less DAB staining than WT seedlings. In this case, the staining was not significantly different from staining in control seedlings not treated with MV (#2, $P = 0.2957$; #5, $P = 0.1257$) (Figure 3, D).

As an orthogonal approach, MV-induced ROS production was detected with 2,7-dihydrodichlorofluorescein diacetate (H$_2$DCF-DA) and quantified as fluorescence intensity per leaf area (Figure 3, E). While for most genotypes treatment with MV caused an increase in fluorescence the most pronounced increase in fluorescence was observed in gstu7 seedlings. Consistent with the earlier experiments, constitutive expression of GSTU7 in the gstu7 background was sufficient to revert the phenotype and limit the fluorescence to values observed in WT seedlings (Figure 3, E).

To better understand if the sensitivity of gstu7 to photo-oxidative stress is linked to an altered level of antioxidant
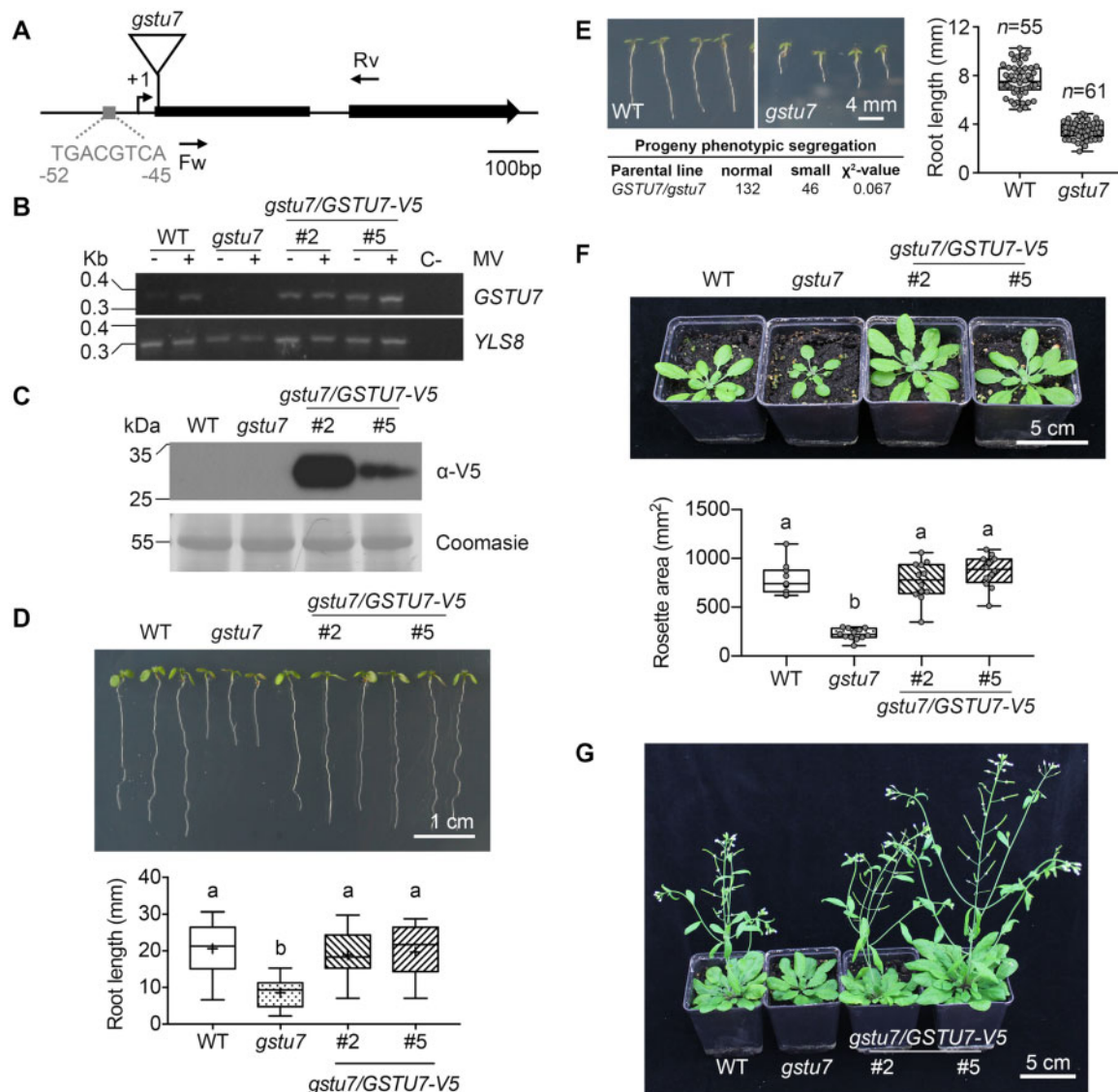
Figure 2 Phenotypic characterization of the Arabidopsis *gstu7* mutant and *gstu7/GSTU7-V5* complemented lines. A, Scheme of the *GSTU7* gene indicating the site of T-DNA insertion in the *gstu7* mutant line (SALK_086642). The TGA-box (gray) is around 50 bps upstream of the transcription start site (+ 1). Forward (Fw) and reverse (Rv) primer binding sites used for mRNA quantification are indicated. B, Quantification of *GSTU7* transcripts in 2-week-old WT, *gstu7*, and two *GSTU7* overexpression lines floated for 24 h in liquid MS medium alone (−) or supplemented with 50µM MV (+). As a negative control for the PCR, a reaction without cDNA was added (C−). A fragment of the *YLS8* housekeeping gene was amplified as a reference. C, Immunoblot analysis of GSTU7 using an antibody against the V5 tag of the complement. Twenty micrograms of protein were loaded per lane. To verify even loading, the membrane was stained with Coomassie Blue (lower panel). D, Growth phenotype of 1-week-old seedlings. Photographs (upper panel) and quantification of the primary root length (lower panel), n = 24–35. E, Segregation of *gstu7*-linked short root phenotype. WT and *gstu7* seedlings were grown vertically on plates and analyzed for their root length 5 d after germination. Segregation of a backcross resulted in a short root:normal WT root ratio of 1:3, n = 55–61. F, Rosette phenotypes of soil grown plants 4 weeks after germination, n = 12. G, Appearance of *gstu7* and complemented lines 7 weeks after germination. For box plots in D, E, and F, Box = interquartile range between the lower and upper quartiles, center line = median, + = mean, whiskers = min and max values. Statistical analyses for D, E, and F were performed using ANOVA with Fisher's LSD test. Different letters indicate statistically different groups ($P < 0.05$).

capacity, GPOX activity was measured in protein extracts from WT, *gstu7*, and the complemented lines after a 4-h incubation in MV-containing solution. For all tested genotypes, MV consistently caused a decrease in GPOX activity. Surprisingly, protein extracts from *gstu7* plants treated only with water contained less GPOX activity compared with WT or the complemented lines (Supplemental Figure S3, A). The

diminished GPOX activity inversely corresponds with higher levels of lipid peroxides quantified as malondialdehyde (MDA) equivalents (Supplemental Figure S3, B). After treatment with MV both, WT and *gstu7* seedlings contained increased amounts of MDA with values in *gstu7* being significantly higher than in WT. Seedlings constitutively overexpressing *GSTU7* had MDA levels similar to homozygous
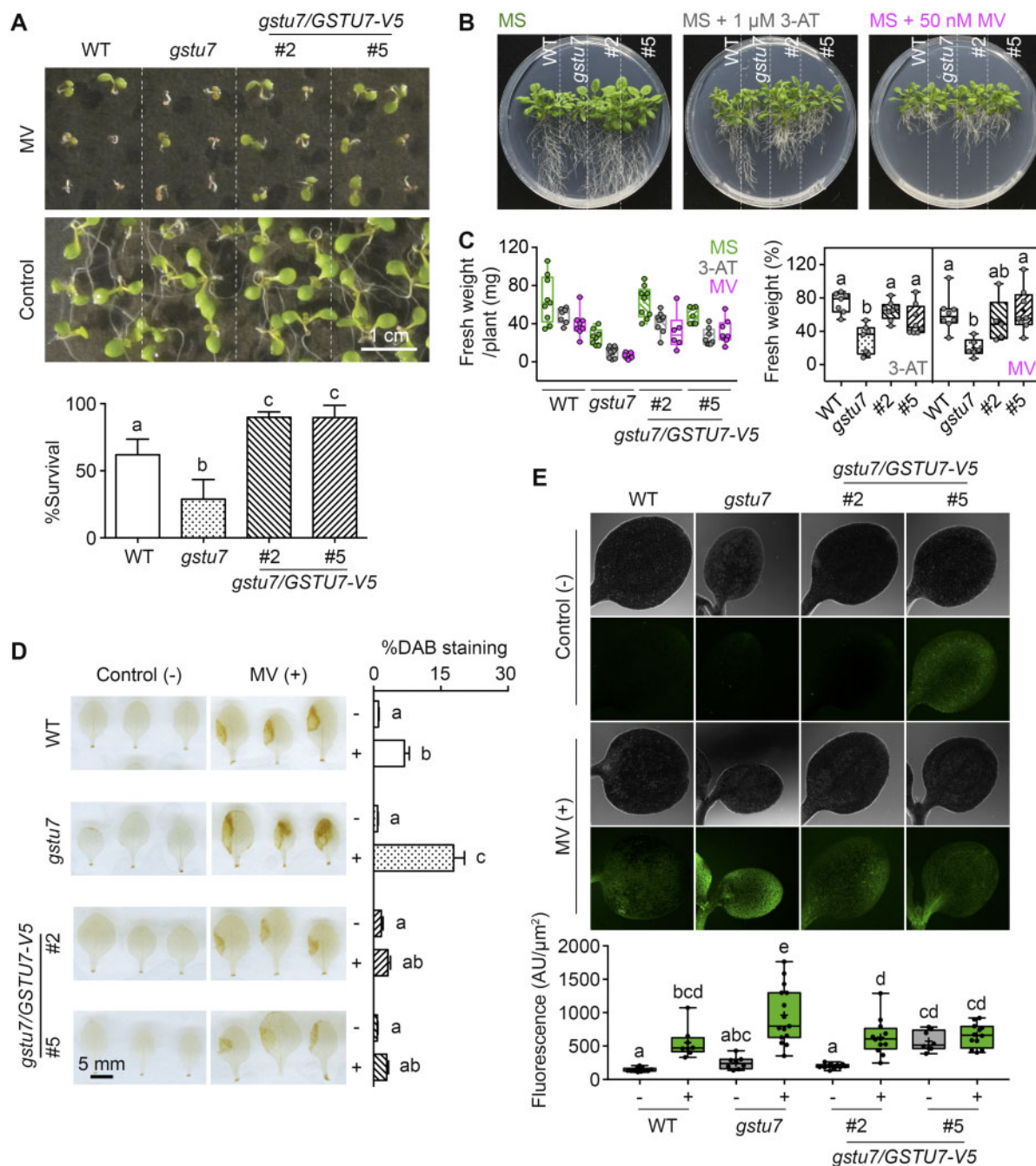
Figure 3 GSTU7 counteracts oxidative stress induced by MV and 3-AT. A, Phenotype of seedlings from WT, *gstu7*, and *gstu7/GSTU7-V5* complemented lines (#2 and #5) grown on MS plates (Control) or MS plates supplemented with 0.1 μM MV. Tolerance of seedlings to MV was measured after 1 week on MV-containing plates as the survival rate, which is the percentage of plants with any green cotyledon over the total number of germinated seeds (*n* = 3, means + SD). B and C, Effect of 3-AT or MV on WT, *gstu7*, and *gstu7/GSTU7* complemented seedlings. Seeds were germinated on MS plates and after 5 d transferred to new MS plates (Control) (B, left) or plates containing either 1 μM 3-AT or 50 nM MV (B, middle and right) on which plants were grown for 17 d. C, Fresh weight of the plants grown in MS or MS supplemented with 1 μM 3-AT or 50 nM MV (C, left plot) and the percentage of fresh weight of 3-AT or MV-treated plants relative to non-treated control plants (C, right plot), *n* = 7–8. D, Accumulation of H_2O_2 in primary leaves exposed to MV. A 2 μL drop of 30 μM MV (+) or water (Control, −) was placed on the leaf surface of plants with different genotypes. Subsequently, the plants were kept under constant light for 24 h before H_2O_2 accumulation was evaluated by staining with DAB. The intensity of DAB staining was quantified as the stained leaf area relative to the whole leave area (% DAB staining) (*n* = 9, means + SD). E, ROS accumulation in cotyledons of 7-d-old seedlings floated for 4 h in 100 μM MV (+) or water (control, −) under constant light. After the treatment, seedlings were stained for 30 min with 25 μM H_2DCF-DA and imaged by confocal microscopy. Fluorescence was collected between 505 and 530 nm after excitation with 488 nm (upper panel). Signal intensity was quantified using FIJI and expressed as intensity per μm² of leaf area (lower panel) (*n* = 8–15). Statistical analyses were performed by ANOVA with Fisher's LSD test. Different letters indicate statistically different groups ($P < 0.05$). For all box plots, Box = interquartile range between the lower and upper quartiles, center line = median, + = mean, whiskers = min and max values.

gstu7 but did not show any further MDA accumulation after treatment with MV (Supplemental Figure S3, B).

A similar stress-induced increase in DAB staining was recently reported for *tga256* after exposure to UV-B light (Herrera-Vásquez et al., 2021). Because the respective TGA transcriptions factors control the expression of *GSTU7* (Figure 1, E), we tested whether *tga256* is also more sensitive to MV and whether this sensitivity is mitigated by overexpression of GSTU7. Consistent with the hypothesis, *tga256* mutants showed a survival rate of only about 4% compared with about 45% for the WT on plates containing 0.1 μM MV (Figure 4). Constitutive overexpression of GSTU7 in *tga256* increased the survival to WT level plants and thus rescued the hypersensitivity of *tga256* to MV. Taken together, these results strongly suggest that GSTU7 plays a central role in mitigating the oxidative stress response triggered by MV.

GSTU7 is located in the cytosol and has GPOX activity

In Arabidopsis, most GSTs are predicted to be localized in the cytosol (Supplemental Figure S1). GSTU7 has been found in the Arabidopsis cytosolic proteome (Ito et al.,

Figure 4 GSTU7 rescues *tga256* triple mutants from MV hypersensitivity. Seeds of WT, *tga256*, and *tga256/GSTU7-V5* complemented lines (#1 and #2) (Herrera-Vásquez et al., 2021) were sown on MS plates (control) or MS plates supplemented with 0.1 μM MV. Seedling tolerance to MV was measured after 1 week as the survival rates. Data indicate means + SD from three independent experiments, where for each experiment 30 germinated plants were counted. Statistical analysis was performed using ANOVA with Fisher's LSD test. Different letters indicate different groups ($P < 0.05$).

2011) and a GSTU7-GFP fusion has only been mentioned to be localized in the cytosol (Dixon et al., 2009). To further confirm these findings, we stably expressed a GSTU7-GFP fusion protein in Arabidopsis and visualized the localization on a confocal microscope (Figure 5, A). All images consistently revealed cytosolic localization of the fusion protein. In all observations, the nuclear region was marked by a bright ring surrounding a dim region with low fluorescence indicating that the fusion protein is barred from the nucleoplasm.

Because of the pronounced mitigation of oxidative stress in *GSTU7* overexpressing seedlings (Figure 3, B), the enzymatic activity of GSTU7 was further evaluated in vitro with the recombinant protein and 1-chloro-2,4-dinitrobenzene (CDNB) as an electrophilic substrate for GST activity and with either H_2O_2 or cumene hydroperoxide (CHP) as substrates for a putative GPOX activity (Figure 5, B and C). GSTU25, which has been reported to be the GST with the highest GPOX and GST activities in Arabidopsis (Dixon et al., 2009), was used as a reference. GSTU7 showed a minor GST activity and was outperformed 97-fold by GSTU25 (Figure 5, B). Both GSTU7 and GSTU25 were capable of reducing H_2O_2 with activities between 51.3 and 23.5 nmol NADPH min^{-1} mg^{-1} (Figure 5, C). Activity of GSTU7 toward CHP was 87.3 nmol min^{-1} mg^{-1} and thus in the same order of magnitude as toward H_2O_2. In contrast, GSTU25 revealed a six-fold higher turnover of CHP compared with H_2O_2 (Figure 5, C).

To validate that the GPOX activity of GSTU7 observed in vitro has biological relevance in vivo, we tested whether GSTU7 can complement a yeast mutant deficient in the respective activity. The *gtt1Δ gtt2Δ* mutant in *Saccharomyces cerevisiae* lacks two key GSTs and has been reported to be sensitive to H_2O_2 and organic peroxides (Choi et al., 1998; Collinson and Grant, 2003; Figure 5, D and E). This yeast strain was transformed with either *GSTU7* or an empty vector control. In the absence of exogenous oxidants, transformed and non-transformed cultures showed the same logarithmic growth curves. Supplementing YPD with either 1.5 mM H_2O_2 (Figure 5, D) or 0.09 mM CHP (Figure 5, E) abolished growth of the cultures almost completely. In medium supplemented with H_2O_2, growth resumed only after a lag phase of 10 h. Cells expressing GSTU7 showed an even longer lag phase of 14 h but reached the same density after 24 h (Figure 5, D). Incubation with CHP completely abolished growth of non-transformed cultures while *gtt1Δ gtt2Δ* cells expressing GSTU7 were able to survive and regain growth after 20 h (Figure 5, E). This supports the hypothesis that GSTU7 possesses GPOX activity in vivo, especially toward CHP.

Because selected glutathione peroxidase (GPX) proteins have been shown to act as protein thiol oxidases and thus can be exploited as H_2O_2 sensors (Delaunay et al., 2002; Gutscher et al., 2009), we also tested whether GSTU7 also is capable of transferring the primary oxidation of its catalytic cysteine resulting from peroxide detoxification to roGFP2 as a target protein. In contrast to bovine GPX used as a
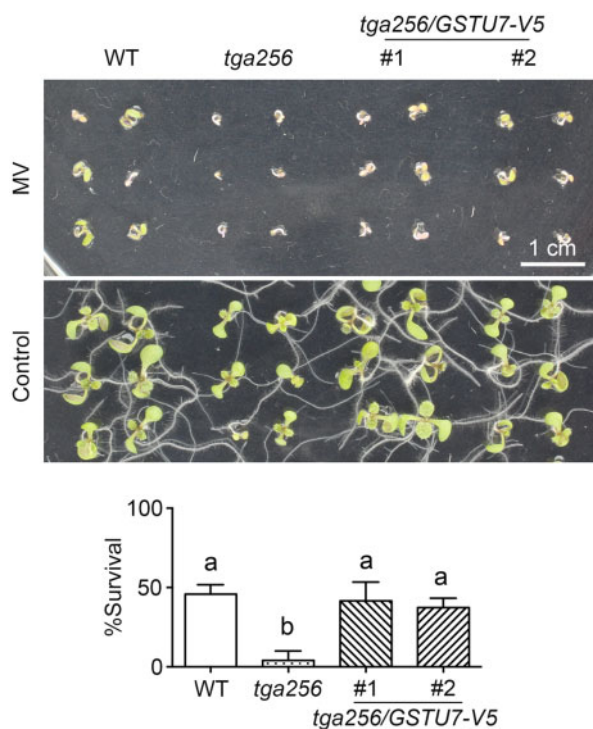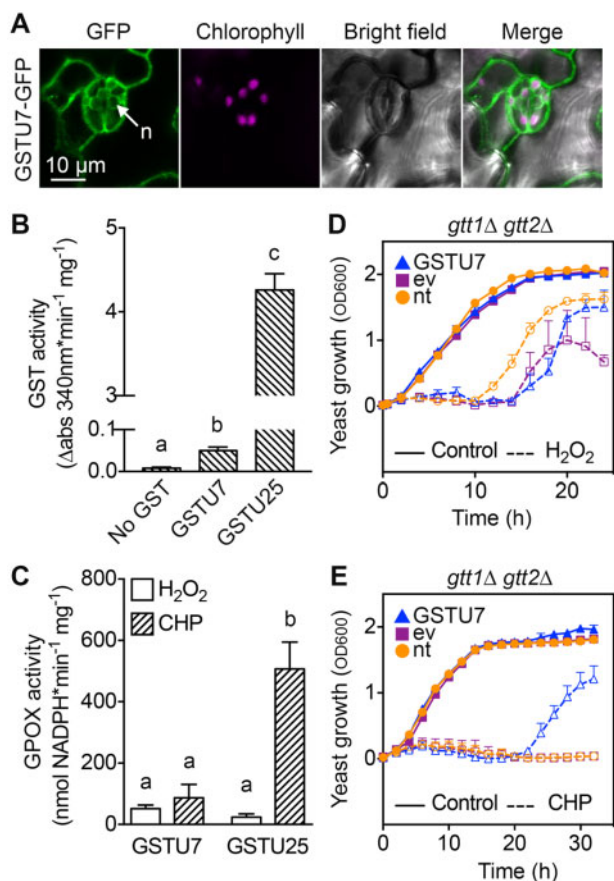
Figure 5 GSTU7 is located in the cytosol and has GPOX activity. A, Confocal microscopy images of Arabidopsis pavement cells and stomata stably expressing $35S_{pro}$:GSTU7-GFP. Panels show GFP fluorescence (λ_{ex} = 488 nm; λ_{em} = 505–530 nm), chlorophyll autofluorescence (λ_{ex} = 488 nm; λ_{em} = 650–695 nm), and transmitted light. Merge images are a projection of the previous channels. The arrow head indicates the nucleus (n) lacking GFP signal. B, GST activity of recombinant GSTU7 and GSTU25 was measured as the conjugation of CDNB with GSH (means + SD of n = 21 for GSTU7 and n = 3 for GSTU25). C, GPOX activity of GSTU7 and GSTU25 upon incubation with H_2O_2 or CHP was measured as consumption of NADPH in a coupled assay with glutathione reductase reducing the produced GSSG (means + SD of n = 4–9). Statistical analysis in panels B and C was performed using ANOVA with Fisher's LSD test. Different letters indicate statistically different groups ($P < 0.05$). D and E, Heterologous expression of GSTU7 in a $gtt1\Delta$ $gtt2\Delta$ yeast strain deficient in the two dominant GSTs. Yeast growth was followed in cells incubated in liquid YPD media (closed symbols, solid line) or YPD supplemented with 1.5 mM H_2O_2 (D) or 0.09 CHP (E) (open symbols; dashed lines). nt, non-transformed; ev, empty vector control. Data represent means + SEM, n = 4.

positive control, GSTU7 was not able to mediate a H_2O_2-dependent oxidation of roGFP2 (Supplemental Figure S4).

GSTU7 protects cytosolic glutathione from MV-induced oxidation

Massive accumulation of ROS induced by MV treatment should also lead to a gradual oxidation of the glutathione redox buffer in the cell. With Grx1-roGFP2 as a fully dynamic probe for the local E_{GSH}, the impact of MV and the role of GSTU7 on the oxidative load in the cytosol can be monitored in living cells over extended time periods. To test whether GSTU7 protects the cell from increased and ultimately deleterious oxidation, we monitored the cytosolic E_{GSH} with Grx1-roGFP2 in vivo, using WT, $gstu7$, and $gstu7$/GSTU7-V5 (#5 line) plants as genetic background and quantified by HPLC the levels of reduced and oxidized glutathione in the non-fluorescent genetic backgrounds. Stable homozygous roGFP2 reporter lines were selected and confirmed to show sufficiently high fluorescence intensities and typical spectral properties of the sensor with two excitations peaks and ratiometric properties using either a confocal microscope or a plate reader (Supplemental Figure S5, A–C).

Changes in the roGFP2 fluorescence ratio triggered by MV treatments were measured in leaf discs of WT, the $gstu7$ mutant, and one of the complemented lines all expressing the Grx1-roGFP2 sensor (Figure 6, A–C). Considering that manipulation of the leaf discs itself can trigger a stress response resulting in an altered redox state (Rosenwasser et al., 2010), leaf samples were initially incubated with 10 mM dithiothreitol (DTT) to attain complete and uniform reduction of the sensor. With this precaution, all measurements started with the sensor at the same level of reduction, serving as the reference point for later ratio normalization. After pre-reduction of the sensor, DTT was removed and leaf discs were incubated either with 100 μM MV or with water as control. WT plants treated with MV showed a gradual increase in the fluorescence ratio over time indicating gradual oxidation of the glutathione pool (Figure 6, A and Supplemental Figure S6). This increase in the fluorescence ratio was more pronounced in $gstu7$ plants (Figure 6, B and Supplemental Figure S6). In contrast, leaves expressing GSTU7 showed no MV-induced oxidation and Grx1-roGFP2 remained almost completely reduced throughout the entire time course of 15 h (Figure 6, C and Supplemental Figure S6).

Glutathione quantification in extracts of all lines confirmed that MV treatment caused a decrease in total glutathione compared with the control conditions. At the same time increased relative amounts of GSSG led to a decrease in the GSH/GSSH ratio, indicating an overall oxidation of the glutathione pool (Figure 6, D and E). This oxidation was slightly more pronounced in $gstu7$ (1.71 ± 0.61) than in the WT (3.64 ± 1.29). In contrast, the line $gstu7$/GSTU7-V5 (#5) that constitutively express GSTU7 showed a consistently higher GSH/GSSG ratio compared with both WT and $gstu7$ (7.27 ± 3.80). The ratio in this case was not significantly different (ANOVA with Fisher's LSD test, P = 0.4639) between MV-treated samples and control seedlings (Figure 6, E).

Discussion

It is well established that GSTU7 is strongly induced under different abiotic stress conditions and that many GSTs are induced by SA and other phytohormones (Marrs, 1996; Sylvestre-Gonon et al., 2019). Our results confirm that SA
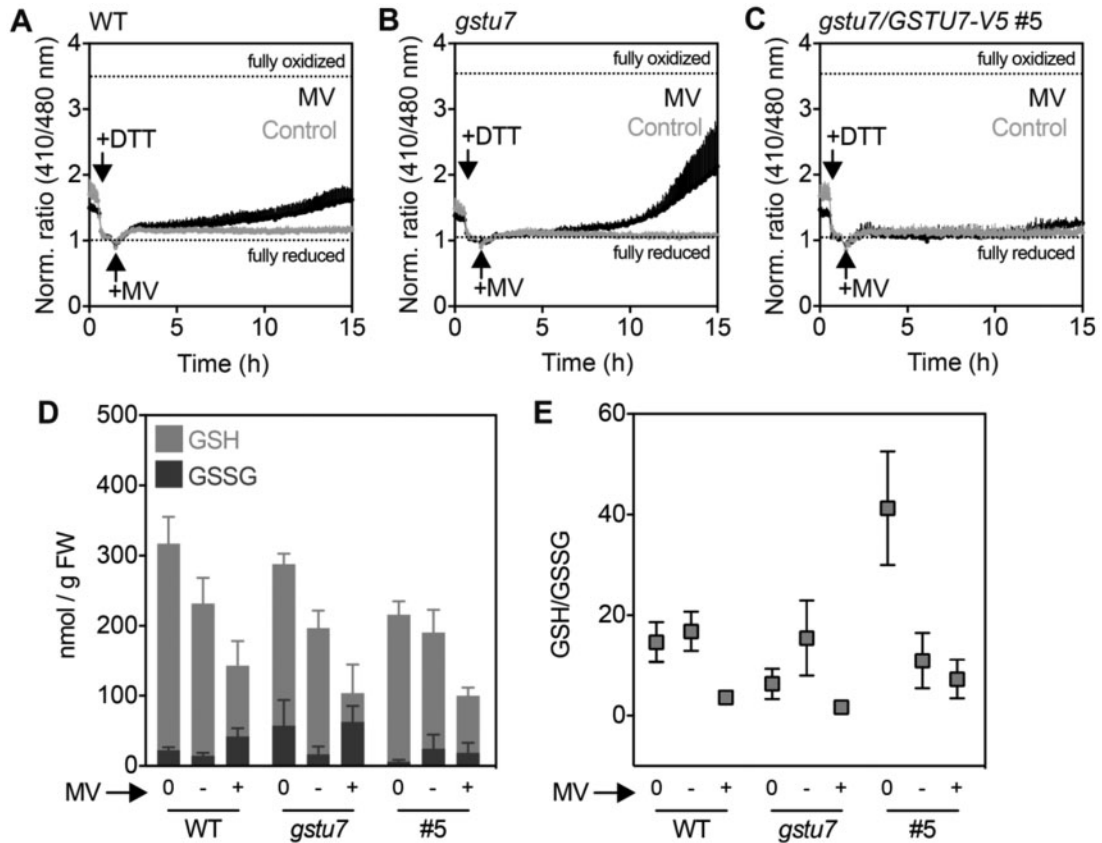
Figure 6 GSTU7 prevents MV-induced oxidation of cytosolic glutathione. A–C, Grx1-roGFP2 was expressed in Arabidopsis WT, *gstu7*, and *gstu7/GSTU7-V5* #5 backgrounds. Leaf discs from stably transformed plants were placed in a 96-well plate and treated with 10 mM DTT to fully reduce the sensor (first black arrow). Subsequently, DTT was removed and the samples were treated with either 100 µM MV or water as control (second black arrow). The redox state of the sensor was followed over time as the ratio between the fluorescence excited at 410 and 480 nm. Ratio values were normalized to the fully reduced sensor after addition of DTT. The dotted lines indicate the ratios for fully reduced and fully oxidized roGFP2 measured at the end of the time course. All data indicate the mean fluorescence + SD of six samples from independent plants. D and E, HPLC analysis of reduced glutathione (GSH) and glutathione disulfide (GSSG) in WT, *gstu7*, and *gstu7/GSTU7-V5* #5 seedlings. Samples were floated in water (–) or 100 µM MV (+) for 15 h under constant light. Samples were also collected before any treatment (0). Data represent means + SD, $n = 3–4$.

induces the expression of *GSTU7* within a few hours of application. In addition, there is also a medium to long-term response resulting in a very pronounced induction of *GSTU7* expression 5 h after irradiation with UV-B or 24 h after application of MV (Figure 1, D). Both transcriptional responses are mediated by class II TGAs but are independent of the endogenous production of SA (Figure 1, D). This indicates that *GSTU7* expression is controlled by at least two separate signaling pathways that are either SA- or TGA256-dependent. A common response to stress situations is the formation of ROS, resulting in secondary responses like lipid peroxidation, which are generally summarized as oxidative stress (Waszczak et al., 2018; Smirnoff and Arnaud, 2019). UV-B triggers an accumulation of H_2O_2 and the finding that GSTU7 can complement the UV-B-sensitive phenotype of *tga256* led to the hypothesis that GSTU7 has an antioxidative function (Herrera-Vásquez et al., 2021). MV treatment is a classical means of inducing oxidative stress in green tissues because MV transfers electrons from PSI to molecular O_2 to form superoxide ($O_2^{\cdot-}$) (Mano et al., 2001). $O_2^{\cdot-}$ is

subsequently converted to H_2O_2, which is not contained in plastids but also reaches the cytosol (Ugalde et al., 2021). Increased susceptibility of *gstu7* null mutants to MV or 3-AT and the more intense MV-induced DAB and H_2DCF-DA staining was completely reverted by overexpression of *GSTU7* (Figure 3). Although it cannot be fully excluded that DAB staining is also responsive to increased level of phenolic compounds (Veljovic-Jovanovic et al., 2002), all evidences presented here are consistent with the hypothesis that more intense DAB staining is a reliable proxy for the increased production of H_2O_2. Even with the confirmatory results from H_2DCF-DA staining, it cannot be distinguished though whether the increased production of H_2O_2 is a primary effect caused by MV-induced photooxidative stress in plastids or a secondary effect due to the increase of intracellular lipid peroxides.

Deletion of GSTU7 resulted in a dwarf phenotype, which was consistently smaller than WT plants throughout its life cycle (Figure 2, D–G). Delayed bolting of *gstu7* is similar to phenotypes of *gstf2* knockdown mutants and *gstu17*

null-mutants (Gong et al., 2005; Jiang et al., 2010; Chen et al., 2012). While loss of GSTU17 expression has no impact on the development of young seedlings under control conditions (Jiang et al., 2010), loss of GSTU7 appears to affect the plant in a more general form resulting in defects in all developmental stages. Conversely, overexpression of a Brassica campestris GSTU closely related to Arabidopsis GSTU24 in Arabidopsis resulted in bigger rosettes, longer primary roots, and an increased number of lateral roots (Kao et al., 2016). At the molecular level, GSTU17 controls plant development by regulating far-red light signaling through interaction with phytochrome A (PHYA) (Jiang et al., 2010). Recently, selective binding of natural products has been shown for GSTU19 and GSTF2 from Arabidopsis (Dixon and Edwards, 2018). Also immobilized recombinant GSTU7 was found to specifically interact with glutathionylated protoporphyrin after HPLC-MS analysis. However, no binding of unique ligands was found after heterologous expression in Nicotiana benthamiana leaves (Dixon and Edwards, 2018).

It is established that GSTUs and GSTFs are subject to complex transcriptional and post-translational regulation in response to infection, abiotic stress, and development (Gullner et al., 2018; Kumar and Trivedi, 2018; Sylvestre-Gonon et al., 2019). The list of abiotic stress factors affecting GST expression has recently expanded to UV-B, which induces the expression of 12 GSTUs including GSTU7 via class II TGA transcription factors (Herrera-Vásquez et al., 2021). Based on these and our own observations, it is tempting to speculate about a function of GSTU7 in ROS metabolism and signaling even though the exact mechanism remains unknown at this stage. Interestingly, the formation of H_2O_2 has been associated with root development and a set of different peroxidases to control the transition from proliferation to differentiation in the root by balancing ROS between root zones (Tsukagoshi et al., 2010; Eljebbawi et al., 2021). It remains unknown though whether the observed growth-inhibitory effects of MV in roots are a secondary effect caused by diminished carbohydrate supply from the shoot or whether it is a primary local effect. Like in mammalian cells, MV is known to also affect the mitochondrial electron transport chain in plants leaving the possibility for an alternative primary source of ROS (Shapiguzov et al., 2019).

Previous studies showed that GSTs mediate detoxification of several classes of herbicides by conjugating GSH to their electrophilic centers (Timmerman, 1989; Prade et al., 1998). Accordingly, plants overexpressing GSTs are frequently more resistant to herbicides (Cummins et al., 1999; Cummins et al., 2013). Furthermore, plant tolerance to the herbicide MV was increased by overexpressing thylakoid ascorbate peroxidase (Murgia et al., 2004), copper–zinc superoxide dismutases (Furusawa et al., 1984; Perl et al., 1993; Aono et al., 1995), as well as different Arabidopsis GSTs, like GSTU4 (Sharma et al., 2014) and GSTU19 (Xu et al., 2016). MV has no electrophilic site for conjugation with GSH and its elimination in plants is thought to take place primarily via photocatalytic degradation

(Moctezuma et al., 1999) while in soil it is degraded through the yeast Lipomyces starkeyi (Carr et al., 1985). In mammals and plants, MV toxicity is associated with the accumulation of lipid peroxides (Misra and Gorsky, 1981; Liu et al., 2009). Consistent with these earlier findings, gstu7 seedlings exposed to MV accumulate more lipid peroxides than WT seedlings (Supplemental Figure S3, B). Efficient elimination of these MV-induced secondary cytotoxic compounds can be assumed to be a critical component of the cellular tolerance to the herbicide and could be a key function of GSTs in the defense response.

In order to generate less-toxic conjugates, GSTs need to interact with both, GSH and the respective toxic electrophilic substrate. Binding of GSH occurs through residues highly conserved among GSTUs, while the second substrate is recognized and bound at the H-sites. The latter are less conserved residues and might explain the diversity of these, toward a diverse array of ligands (e.g. xenobiotics, herbicides, or hormones) (Sylvestre-Gonon et al., 2019). To explore putative H-sites in GSTU7, a sequence alignment was made with Arabidopsis GSTUs from each cluster within the TAU subfamily plus other plant GSTUs with known substrates or resolved crystal structures (Supplemental Figure S1, B). The alignment revealed that the H-site of GSTU7 contains a Met–Trp–Ala motif that is also present in OsGSTU4 from rice. The overexpression of OsGSTU4 in Arabidopsis has proven to generate more tolerant plants toward salt stress and MV-induced photooxidative stress, while in silico characterization led to the hypothesis that OsGSTU4 might detoxify the herbicide metsulfuron (Sharma et al., 2014; Amador et al., 2020). These results together suggest a conserved function of distinct TAU GSTs and may provide leads for further analysis.

GSTs are mostly located in the cytosol, with only three family members predicted to be localized in plastids (Supplemental Figure S1). We confirmed the cytosolic localization of GSTU7 through stable expression and visualization of GSTU7-GFP fusion proteins in Arabidopsis (Figure 5, A). In line with observations by (Dixon et al., 2009) we found GSTU7 being excluded from the nucleus. But in the absence of any obvious nuclear exclusion signal it is not clear how this exclusion is mediated or whether it is a consequence of the GFP fusion, which results in a larger fusion protein of 53 kDa. Indeed, GSTU7 might form homo- or heterodimeric protein complexes with molecular mass higher than 100 kDa, which is well above the size exclusion limit of about ~40 kDa of nuclear pores for passive transport (Tamura and Hara-Nishimura, 2014).

Most GSTUs have been reported to have a GPOX activity with CPH as substrate (Dixon et al., 2009). This includes GSTU7, which, however, is among the family members with the lowest GPOX activity. Our data confirm this low activity also in comparison to the highly active GPOX GSTU25. Similarly, the about 100-fold lower GSTU7 activity toward CDNB as an electrophilic substrate compared with GSTU25 largely confirms the relative activities measured by Dixon et al. (2009) (Figure 5). Nonetheless, GPOX activity toward H_2O_2 in total protein extracts proved to be diminished in

gstu7 (Supplemental Figure S3). As a different approach, we tested for thiol oxidase activity of GSTU7 with roGFP2 as the reporting target protein for oxidation. All these attempts with recombinant GSTU7, however, failed and thus do not provide a clear lead for further biochemical characterization of the enzymatic activity (Supplemental Figure S4). This leaves us with the conundrum of an enzyme preventing cells from severe oxidation induced by MV or UV-B and a lack of biochemical information. A possible limitation of the biochemical in vitro assays may be that GSTs tend to form homo- or heterodimeric protein complexes (Cummins et al., 1997; Dixon et al., 1997; Gronwald and Plaisance, 1998), which may not occur with recombinant proteins. In this situation, we thought to get access to the function of GSTU7 by testing its activity in vivo. In a previous study that aimed at functionally characterizing the large family of plant GSTs for their role in fungicide detoxification, almost all Arabidopsis GSTs were expressed in a GST-deficient yeast strain (*gtt1Δ gtt2Δ grx1Δ grx1Δ tef4Δ*), which is hypersensitive to fungicides and CDNB (Krajewski et al., 2013). Complementation of this yeast strain with different GSTs, including GSTU7, resulted in increased tolerance toward fungicides. Here, overexpression of GSTU7 in the GST-deficient yeast strain *gtt1Δ gtt2Δ* conferred at least partial tolerance to CHP, which further supports the notion that GSTU7 may be involved in lipid peroxide detoxification. roGFP2 is extremely sensitive to even minor increases in glutathione disulfide (GSSG) during detoxification of peroxides with GSH as electron donor (Marty et al., 2009). The completely abolished MV-induced oxidation in GSTU7 overexpressor plants strongly argues against the hypothesis for a GPOX activity and rather suggests that GSTU7 acts earlier in the pathway between MV and H_2O_2 accumulation. The fact that GSTU7 also rescues *tga256* mutants from UV-B stress (Herrera-Vásquez et al., 2021) strongly argues for a direct role of GSTU7 in peroxide detoxification.

Overall, our results reveal the importance of Arabidopsis GSTU7 as a protective enzyme for cellular detoxification, development, and the antioxidant response to herbicides, such as MV. Whether the identified phenotypes in development and under stress situations are dependent on different molecular functions of GSTU7 or whether these functions converge to the same mechanism remains unknown. Thus, further studies are needed to elucidate the mechanistic properties of GSTU7 in plant growth and during MV-induced oxidative stress. Beyond future work on the mechanism, the current findings may also open new research possibilities for breeding of more stress-tolerant plants, in which over-expression of *GSTs* may contribute to overcoming present and future challenging environmental conditions that would lead to formation of ROS in plants.

Materials and methods

Plant material and growth conditions

Arabidopsis (*A. thaliana* [L.] Heynh.) WT, *sid2-2* (Wildermuth et al., 2001), *tga256* (Zhang et al., 2003), *gstu7* (SALK_086642C, ABRC, characterized in this work), *tga256/GSTU7-V5* lines #1 and #2 (Herrera-Vásquez et al., 2021), and *gstu7/GSTU7* lines #2 and #5 (obtained in this work) were in Columbia (Col-0) background. Seeds were surface sterilized with 70% ethanol and rinsed three times with sterile deionized water. Clean seeds were sown on plates with $0.5\times$ Murashige and Skoog (MS) growth medium (Murashige and Skoog, 1962) (Phyto Technology Laboratories, Shawnee Mission, KS) supplemented with 1 g L^{-1} sucrose and 3 g L^{-1} phytagel (Sigma, Steinheim, Germany) or 8 g L^{-1} agar (Winkler, Santiago, Chile). Plates were incubated in a growth chamber under a long day regime (16-h light, 100 µmoles m^{-2} s^{-1}, at 22°C ± 2°C; 8-h dark at 18°C± 2°C). For experiments with leaf discs, 5-d-old seedlings were transferred to Jiffy-7 peat pellets (Jiffy, Oslo, Norway) and grown under the same controlled conditions for 4–5 weeks. Leaves were excised using a 7-mm-diameter cork borer.

Plant treatments for gene expression analysis

Treatments to evaluate gene expression were performed on 2-week-old seedlings grown under a long-day regime. Whole seedlings were collected at the indicated time points, frozen in liquid nitrogen, and stored at −80°C until processing. For SA treatments, seedlings were floated on a solution of 0.5 mM sodium salicylate (Sigma), $0.5\times$ MS, 1% (w/v) sucrose liquid medium or $0.5\times$ MS, and 1% (w/v) sucrose liquid medium as control. Treatments with MV (Sigma) were performed with seedlings floated on a solution of 50 µM MV, $0.5\times$ MS, 1% (w/v) sucrose liquid medium or using $0.5\times$ MS, and 1% (w/v) sucrose liquid medium as a control, for the indicated time points. MV stock aliquots (10 mM, dissolved in deionized water) were stored at −20°C in the dark and used within 1 month after the preparation. UV-B treatment was performed in a chamber equipped with two F8T5 UVP3400401 fluorescent tubes ($\lambda = 306$ nm) (USHIO, Cypress, CA) at a distance of 53 cm from the samples, irradiating with an intensity of 0.220 mW cm^{-2}. As a control, a 2-mm-cellulose acetate polyester was used to filter UV-B radiation.

Gene expression analysis

Total RNA was extracted with TRIzol reagent (Invitrogen, Carlsbad, CA) following the manufacturer's instructions. cDNA was synthesized from 2 µg of total RNA with the MMLV kit (Promega, Madison, WI). Semi-quantitative PCR was performed within the linear amplification phase using a recombinant Taq Polymerase (Invitrogen) amplifying a fragment of 323 bp of the coding sequence of *GSTU7* and a fragment of 294 bp of the *YLS8* housekeeping gene. Quantitative PCR was done using the Brilliant III Ultra-Fast SYBR Green Master mix (Agilent Technologies, Santa Clara, CA) in an AriaMx (Agilent Technologies) or an MX3000P instrument (Stratagene San Diego, CA). Expression levels of *GSTU7* were calculated as fold-change to the *CLATHRIN ADAPTOR COMPLEX* gene (*CLA*), for SA and MV treatments,

or to *YSL8* for UV-B treatments. Primer sequences are listed in Supplemental Table S1.

Oxidative stress tolerance assay and ROS detection

MV tolerance assays were performed according to Laporte et al. (2012), with the following modifications. Surface sterilized seeds were stratified for 48 h in the dark at 4°C and then sown on MS-Phytagel plates supplemented with 0.1 μM MV. After 1 week, tolerance to MV was measured as survival rate that is the percentage of green seedlings/cotyledons compared with the total number of germinated seeds. For 3-AT (3-Amino-1,2,4-triazole, 3-AT) (Sigma–Aldrich) tolerance, seedlings were grown on MS-Agar plates for 5 d and then transferred to new MS-Agar plates supplemented with 1 μM 3-AT or MS-Agar plates as control. Subsequently, plants were allowed to grow for another 17 d before analysis for which plates were photographed and the fresh weight of individual plants determined. 3-AT tolerance was determined for each genotype as the percentage of fresh weight after 3-AT treatment relative to the weight under control conditions.

To evaluate the mitigation of MV-induced oxidative damage by GSTU7, either 2 μL of a 30 μM MV solution or 2 μL of water were placed as a single drop on the adaxial side of leaves of 2-week-old seedlings grown on plates. After a 24-h incubation period in constant light, the accumulation of H_2O_2 was measured after staining with DAB (Sigma) according to Daudi et al. (2012). Leaves were detached and placed in six-well plates with 2 mL of staining solution. After a 5 min vacuum-infiltration, samples were incubated with constant orbital agitation for 6 h in the dark or until staining was visible. Chlorophyll was removed by boiling in 80% (v/v) ethanol and subsequent rinsing with distilled water. To assess the relative labeling intensity and enable a direct comparison between leaves from different genotypes and MV-treated and non-treated leaves, all stained leaves together were mounted in 20% glycerol between two SDS-page glass plates and documented with an Epson V850 Pro scanner. Quantification of the staining was performed using the FIJI software (Schindelin et al., 2012). Images were first converted to 8-bit grayscale dark pixels representing DAB staining. Subsequently, an arbitrary threshold was defined to mask out all obviously DAB-stained areas, that is pixels with most intense staining and hence the lowest gray values on the 8-bit grayscale. In the current experiments, this accounted to 3% of all pixels in the whole scan. The area of the masked pixels for each leaf was then compared with the whole lamina size of the respective leaf to get a relative measure of the DAB staining that allowed direct comparison of all different leaves and treatments.

MV-dependent ROS production was also tested in 7-d-old seedlings immersed for 4 h in imaging buffer (10 mM MES, 10 mM $MgCl_2$, 10 mM $CaCl_2$, 5 mM KCl, pH 5.8) supplemented with 100 μM MV or just buffer as control and exposed to constant actinic light to induce photooxidative stress according to Ugalde et al. (2021). After the treatment, the seedlings were carefully transferred to a 25 mM H_2DCF-DA (Sigma–Aldrich) staining solution prepared in 10 mM Tris–HCl (pH 7.4) buffer. Samples were incubated for 30 min and rinsed three times with Tris buffer before being imaged with a 5× lens (EC-Plan-Neofluar, NA 0.16). Fluorescence resulting from H_2DCF-DA labeling was collected at 505–530 nm prior excitation with 488 nm. Fluorescence intensity was quantified per mm^2 of cotyledon using the FIJI software and expressed as arbitrary units of fluorescence per mm^2.

Bacterial infections and ion leakage

Pseudomonas syringae pv. tomato DC3000 avirulent strains expressing the AvrRpt2 effector were grown at 28°C under constant shaking on King B media supplemented with 50 μg/mL kanamycin and 50 μg/mL rifampicin. Cells were collected by centrifugation at 5,000 g for 7 min and washed twice with sterile water before resuspension in sterile 10 mM $MgCl_2$ solution to a final concentration of 1×10^5 cfu/mL. Two-week-old plants grown in plates were inoculated by flooding (Ishiga et al., 2011) with 30 mL of the bacterial suspension for 3 min. After inoculation, the bacterial suspension was discarded and the plants were incubated in long day conditions for 72 h. Pathogen-induced cell death was measured as the ions leaked from the sample after infection. The aerial part of three infected plants was pooled and incubated for 20 min in 6 mL of deionized water under constant agitation. Water was discarded and samples were incubated in 6 mL of fresh deionized water for 16 h under constant agitation. The released ions were measured as conductivity using a Twin Cond B-173 conductometer (Horiba, Tokyo, Japan). The conductivity was expressed relative to the conductivity measured for autoclaved samples and presented as the ion leakage (%).

Cloning and plant transformation

For complementation of *gstu7* and transient expression of the GSTU7-GFP fusion protein, the constructs $UBQ10_{pro}$:*GSTU7-V5* and $35S_{pro}$:*GSTU7-GFP* were used, respectively. To obtain these constructs, a fragment of 681 bp corresponding to the full CDS of *GSTU7* (stop codon excluded) was amplified by PCR using the forward and reverse pEN-GSTU7-CDS primers (see Supplemental Table S1 for sequences). The fragment was purified using a NucleoSpin kit (Macherey-Nagel, Düren, Germany) and cloned into the pENTR/SD/D-Topo vector (Invitrogen) following the manufacturer's instructions. The entry clone pEN-GSTU7 was recombined into the pB7m34gW destination vector (Karimi et al., 2002), together with pDONR-pUBQ and pDONR-V5-His (Herrera-Vásquez et al., 2021) which contained the sequences for the ubiquitin 10 promoter ($UBQ10_{pro}$) and V5 tag ($UBQ10_{pro}$:*GSTU7-V5*), respectively. For subcellular localization, the CDS of *GSTU7* cloned in the pEN-GSTU7 was fused to the GFP fluorescent protein sequence by recombination with the pK7FWG2.0 binary vector (Karimi et al., 2002), generating the $35S_{pro}$:*GSTU7-GFP* construct.

$UBQ10_{pro}$:*GSTU7-V5* and $35S_{pro}$:*GSTU7-GFP* constructs were transformed into *Agrobacterium tumefaciens* strain

C58C1 and stable Arabidopsis transgenic lines were generated by floral dip (Clough and Bent, 1998). Transformed seeds were surface-sterilized and selected on plates with $0.5\times$ MS solid medium supplemented with 10 µg mL^{-1} ammonium glufosinate (Sigma) for $UBQ10_{pro}$:GSTU7-V5 or 50 µg mL^{-1} kanamycin for $35S_{pro}$:GSTU7-GFP.

To express the Grx1-roGFP2 redox sensor in the different genetic backgrounds, gstu7 was crossed with a WT plant expressing Grx1-GFP2 in the cytosol, and the complemented line gstu7/GSTU7 #5 was transformed by floral dip with a plasmid containing the $UBQ10_{pro}$:Grx1-roGFP2 construct.

For protein purification, the plasmid pETG-GSTU7-His was generated. For this purpose, the CDS of GSTU7 was amplified by PCR with the forward and reverse pDon-GSTU7-CDS primers carrying the respective attB recombination sites (see Supplemental Table S1 for sequences); the fragment was then purified and cloned into the pDONR201 entry vector (Invitrogen) following the manufacturer's instructions and recombined with the pETG10A vector, adding a C-terminal His$_6$ tag to GSTU7. In parallel, the entry vector, pDONR-GSTU7, was recombined with the binary vector pAG415GPD-ccdB-HA (a gift from Susan Lindquist, Addgene plasmid # 14242) for GSTU7 expression in S. cerevisiae. All constructs were verified by sequencing.

Yeast complementation and growth

The S. cerevisiae mutant gtt1::TRP1 gtt2::URA3 (gtt1Δ gtt2Δ), in the genetic background W303 (Choi et al., 1998; Collinson and Grant, 2003), was transformed either with the empty vector (ev) pAG415GPD-ccdB-HA or a version harboring GSTU7 according to Gietz and Woods (2002). Cells were grown overnight at 30°C under constant agitation in 15 mL of synthetic SD medium without leucine (2% [w/v] glucose, 0.67% [w/v] yeast nitrogen base, 0.13% [w/v] yeast synthetic drop-out supplement [Sigma], 0.004% [w/v] L-histidine, 0.004% [w/v] L-tryptophane, 0.002% [w/v] L-uracil). Aliquots of the saturated cultures were incubated for 2 h in 15 mL of fresh medium until they reached exponential growth and then diluted with YPD media (20 g L^{-1} tryptone/peptone, 10 g L^{-1} yeast extract) to a final OD$_{600}$ = 0.1. Oxidative conditions were generated with H$_2$O$_2$ or CHP, added to the indicated final concentrations. Growth rates were measured as absorbance at 600 nm on a POLARstar plate reader (BMG Labtech, Ortenberg, Germany) in a final volume of 200 µL at 27.5°C.

Protein extraction and immunodetection

Protein extracts were obtained from 2-week-old frozen seedlings by grinding the material in a microfuge tube with a plastic pestle. The resulting powder was suspended in lysis buffer (50 mM sodium phosphate buffer, pH 7.5–8.0, 150 mM NaCl, 0.2% [w/v] IGEPAL, and 5 mM EDTA) and supplemented with a protease inhibitor cocktail (Roche Diagnostics, Mannheim, Germany). Samples were centrifuged at 2,350 g for 10 min at 4°C and the supernatant was collected. Protein concentration was determined by the Bradford method, using the BioRad Protein Assay (Bio-Rad

Laboratories, Inc., CA, USA), and samples were stored at −80°C.

Immunoblot was performed according to Seguel et al. (2018). Total protein samples (30 µg) were resolved in 12% (w/v)-SDS-PAGE and transferred to Immobilon PVDF membranes (Millipore, Burlington, MA) in a semi-dry electroblotting apparatus (Bio-Rad). Membranes were blocked overnight at 4°C in a solution of 5% (w/v) skimmed milk powder prepared in a PBS-T phosphate buffer (137 mM NaCl, 2.7 mM KCl, 10 mM Na$_2$HPO$_4$, 2 mM KH$_2$PO$_4$ and 0.1% [v/v] Tween-20). GSTU7-V5 fusion protein was detected with anti-V5 mouse monoclonal antibody (1:5,000 dilution, from Invitrogen #R96025) and a peroxidase-conjugated anti-mouse secondary antibody (1:10,000 dilution from KPL, Gaithersburg, MD #074-1806). GSTU7-V5 fusion was visualized with a 1:1 mix of SuperSignal West Pico and SuperSignal West Femto chemiluminescent substrates (Thermo Fisher Scientific, Waltham, MA).

Protein purification and enzyme assays

A culture of Escherichia coli strain BL21 harboring pETG10A-GSTU7 was grown in LB medium supplemented with 100 µg mL^{-1} ampicillin at 37°C with constant shaking. Fresh cultures were prepared from saturated aliquots and grown until cells reached an OD$_{600}$ of 0.6–0.8. GSTU7-His expression was induced by incubating the cells for 24 h with isopropyl β-D-1-thiogalactopyranoside (IPTG) in a final concentration of 0.5 mM and 200 µL of anti-foaming solution (Sigma), with constant shaking at 22°C. Cells were collected by centrifugation at 4,000 g for 15 min at 4°C and the pellet was suspended in a buffer (100 mM Tris–HCl, pH 8.0, 150 mM NaCl, 0.5 mM PMSF) supplemented with 5 mg L^{-1} DNAse I and 0.5 g/L lysozyme (Roche Diagnostics). Cells were disrupted by sonication (3 × 2 min, 40% power output, 50% duty cycle, in a SONOPULS Ultrasonic Homogenizer HD 2200, Bandelin, Berlin, Germany). The lysate was centrifuged at 19,000 g for 20 min at 4°C and the supernatant filtered through a sterile filter with 0.22 µm nominal size. The filtered fraction was loaded onto a Ni-NTA HisTrap column (GE Healthcare, Little Chalfont, UK) using a peristaltic pump at a rate of 1 mL min^{-1}. Proteins were eluted from the column with a 10–200 mM imidazole gradient (100 mM Tris–HCl, pH 8.0, 200 mM NaCl) using an ÄKTA Prime Plus chromatography system (GE Healthcare, Chicago, IL). Fractions were collected and stored at 4°C and the presence of GSTU7-His protein was confirmed by analyzing the collected fractions by SDS-PAGE.

GPOX enzyme activity was measured using a GR-coupled protocol adapted from Navrot et al. (2006) and expressed as the decrease in absorbance of NADPH at 340 nm in the presence or absence of a peroxide substrate. A final concentration of 10 µM recombinant GSTU7 protein, or no protein as the basal line, was incubated with 5 M yeast GR1, 400 µM NADPH, and 500 µM GSH as the electron donor. The assays were carried out in a final volume of 100 µL in assay buffer (100 mM Tris–HCl, pH 7.4, 5 mM EDTA) where the substrates, H$_2$O$_2$, or CHP, were automatically injected to a

final concentration of 200 μM. The absorbance was recorded at 340 nm in a POLARstar plate reader. The test thiol oxidase activity of GSTs, 10 μM of purified GSTU7 were incubated with 1 μM of purified roGFP2 and 4 mM of either H_2O_2 or CHP. Bovine GPX (Sigma) was used as a control. Oxidation of roGFP was followed on the plate reader exciting at 390 ± 5 and 480 ± 5 nm, and collecting the fluorescence from both channels at 520 ± 5 nm.

GPOX activity was determined as well in protein extracts from Arabidopsis plants. For this, 2-week-old WT, *gstu7*, *gstu7/GSTU7-V5* #2, and #5 plants were incubated in deionized water or 100 μM MV for 4 h under constant actinic light. After treatment, 500 mg of tissue was collected and homogenized in liquid N_2 using a mortar and pestle. The grounded tissue was resuspended in 1 mL cold lysis buffer and centrifuged at 16,000 g for 20 min at 4°C, saving the supernatant in a new tube. After quantification, 60 μg of total protein extract was resuspended in final 500 μL of reaction mix (50 mM phosphate buffer pH 7.0, 1 mM GSH, 0.15 mM NADPH, and 5 U of glutathione reductase). In addition, 10 mM H_2O_2 was added immediately before the measurements were performed. GPOX activity was measured as the decrease in absorbance at 340 nm during the first minute of the reaction after H_2O_2 addition.

GST enzyme activity was measured as the conjugation of GSH to CDNB. The increase of GS-CDNB conjugate was followed as an increase in absorbance at 340 nm in a POLARstar plate reader. For preparing the stock solutions, 200 mM GSH was dissolved in assay buffer (100 mM Tris–HCl, pH 7.4, 5 mM EDTA) and 100 mM CDNB was dissolved in 96% (v/v) ethanol. The assay mix was prepared by adding 100 μL of each stock solution to 9.8 mL of assay buffer before use. For the plate reader measurements, 195 μL of assay buffer was added to 5 μL of diluted recombinant GSTU7 protein and measured for 10 min after 10 s of orbital agitation at 200 rpm. All measurements were done in triplicates with three different batches of purified protein.

Lipid peroxidation quantification

MV-induced lipid peroxidation was determined as the accumulation of MDA equivalents by the thiobarbituric acid reactive substances (TBARS) assay. For this 3-week-old WT, *gstu7* and *gstu7/GSTU7-V5* #2 plants were floated in distilled water or 100 μM MV for 16 h under constant actinic light. After treatment around 150 mg of tissue was ground in liquid N_2 and the homogenized, resuspended in 1 mL of precooled 0.1% (v/v) TCA. Samples were centrifuged at a maximum speed for 10 min at 4°C, and the supernatant was placed in a new tube on ice. About 300 μL of supernatant was added to a tube with 1 mL of reaction mix (20% [v/v] TCA, 0.5% [v/v] TBA) and to a no TBA mix (20% [v/v] TCA) for later background subtraction (Landi, 2017). The reaction was incubated for 30 min at 95°C, cooled down in ice, and centrifuged again at maximum speed for 10 min at

4°C. From the supernatant, MDA was measured as the absorbance at 532 nm and its concentration was calculated using MDA's extinction coefficient = 155 mM^{-1} cm^{-1}.

Confocal microscopy

Arabidopsis plants stably expressing the 35Spro:GSTU7-GFP construct were grown in MS-Agar plates for 4 d and imaged on a confocal laser scanning microscope (Zeiss LSM 780, connected to an Axio Observer.Z1; Carl Zeiss Microscopy, Jena, Germany) using a 40× lens (C-Apochromat 40×/1.2 W Korr). GFP and chlorophyll were excited at 488 nm and fluorescence emission was collected at 499–553 and 630–691 nm, respectively. Ratiometric imaging and analysis of WT and mutant lines harboring the Grx1-roGFP2 sensor were performed as described by Attacha et al. (2017) utilizing a custom-written MATLAB script (Fricker, 2016).

Monitoring of roGFP2 fluorescence in leaf discs

Fluorescence of the Grx1-roGFP2 sensor expressed in 4–5-week-old WT, mutant, and complemented lines was initially confirmed in a stereomicroscope (M165 FC, Leica, Wetzlar, Germany) equipped with a GFP filter (470 ± 40 nm excitation and 525 ± 50 nm emission) and documented with the attached camera (DFC425 C, Leica). Leaf discs were cut from positive fluorescent plants using a 7-mm cork borer and placed with the abaxial side up in the bottom of transparent Nunc 96-wells plates (Sigma).

For spectral measurements, leaf samples were excited in the range of 360–496 nm with a step width of 1 nm and the emission was collected at 520 nm using a CLARIOstar plate reader (BMG Labtech). Non-fluorescent samples of each genotype and treatment were used to subtract the basal background fluorescence.

Ratiometric measurements of Grx1-roGFP2 in leaf samples were performed in a POLARstar plate reader equipped with two excitation filters, 410 ± 5 nm for the peak of the oxidized roGFP, and 480 ± 5 nm for the peak of the reduced roGFP; the emitted fluorescence was collected at 520 ± 5 nm. Samples were equally treated in 200 μL of final volume and the fully reduced and oxidized treatments were performed using a solution of 10 mM DTT or 5 mM 2,2′-Dipyridyldisulfide (DPS), respectively.

Leaf samples were treated with DTT to fully reduce the sensor, then rinsed twice with distilled water, and treated with 200 μL of 100 μM of MV or distilled water as control. Fluorescence was measured every 210 s for over 15 h at a constant temperature of 25°C. To assess the dynamic range of the sensor, at the end of each experiment the probe was fully reduced and then fully oxidized by discarding the solution containing MV, and replacing it with 200 μL of 10 mM DTT for 5 min and then replacing it with 200 μL of 5 mM DPS. For every measurement, non-fluorescent samples of each genotype were treated and recorded under the same conditions. These values were later used to subtract autofluorescence. The experiment was repeated six times and,

for each experiment, six leaf discs from independent plants were used for the measurements.

Analysis of low-molecular-weight thiols under oxidative stress

Seeds from WT, *gstu7*, and *gstu7/GSTU7-V5* #5 were surface sterilized and vertically grown on MS-Agar plate for 7 d. Seedlings were harvested and floated in 100 µM MV or distilled water as control, and incubated for 15 h under constant actinic light. After the treatment approximately 30 mg of fresh tissue was collected per replicate and snap frozen in liquid N_2. Sample homogenization and thiol quantification were done as described in Bangash et al. (2019).

Sequence alignment and phylogenetic analysis

Protein sequences were aligned in Jalview (Waterhouse et al., 2009) using the Muscle algorithm with default settings. After manual curation of the sequence alignment, an unrooted phylogenetic tree of Arabidopsis GSTs (SSupplemental Figure S1) was constructed using Bayesian inference with MrBayes (Ronquist and Huelsenbeck, 2003). A graphical representation of the phylogenetic tree was created using the Figtree software (v1.4.2, A. Rambaut, http://tree.bio.ed.ac.uk/software/figtree/).

Accession numbers

All the sequence information in this article is referred to as in the GenBank/EMBL database under the following accession numbers. From *A. thaliana*: AT2g29420 (*GSTU7*), AT1G17180 (*GSTU25*), AT5G06950 (*TGA2*), AT5G06960 (*TGA5*), AT5G06950 (*TGA6*), At5g46630 (*CLATHRIN ADAPTOR COMPLEX*), At5g08290 (*YLS8*), and AT1g74710 (*ICS1/SID2*). From *Saccharomyces cerevisiae*: YIR038C (*GTT1/GST1*) and YLL060C (*GTT2/GST2*).

Supplemental data

The following materials are available in the online version of this article.

Supplemental Figure S1. Phylogenetic analysis of the GST protein family from Arabidopsis.

Supplemental Figure S2. Cellular ion leakage under abiotic and biotic stress.

Supplemental Figure S3. GPOX activity and lipid peroxide accumulation in *gstu7* under MV exposure.

Supplemental Figure S4. roGFP2 thiol oxidation assay.

Supplemental Figure S5. Subcellular localization and spectral properties of the Grx1-roGFP2 sensor in Arabidopsis leaves.

Supplemental Figure S6. Biological replicates for measurement of the glutathione redox state in response to MV in Arabidopsis leaves.

Supplemental Table S1. List of primers used in this work.

References

Alfenito MR, Souer E, Goodman CD, Buell R, Mol J, Koes R, Walbot V (1998) Functional complementation of anthocyanin sequestration in the vacuole by widely divergent glutathione *S*-transferases. Plant Cell **10**: 1135–1149

Amador VC, da Silva EF, Nadvorny D, Maia RT (2020) Possible metsulfuron herbicide detoxification by a *Oryza sativa* L. glutathione *S*-transferase enzyme. Braz Arch Biol Technol **63**: doi: 10.1590/1678-4324-2020180571

Aono M, Saji H, Sakamoto A, Tanaka K, Kondo N, Tanaka K (1995) Paraquat tolerance of transgenic *Nicotiana tabacum* with enhanced activities of glutathione reductase and superoxide dismutase. Plant Cell Physiol **36**: 1687–1691

Attacha S, Solbach D, Bela K, Moseler A, Wagner S, Schwarzländer M, Aller I, Müller SJ, Meyer AJ (2017) Glutathione peroxidase-like enzymes cover five distinct cell compartments and membrane surfaces in *Arabidopsis thaliana*. Plant Cell Environ **40**: 1281–1295

Bangash SAK, Müller-Schüssele SJ, Solbach D, Jansen M, Fiorani F, Schwarzländer M, Kopriva S, Meyer AJ (2019) Low-glutathione mutants are impaired in growth but do not show an increased sensitivity to moderate water deficit. PLoS ONE **14**: e0220589

Basantani M, Srivastava A (2007) Plant glutathione transferases—a decade falls short. Can J Bot **85**: 443–456

Becher M, Talke IN, Krall L, Krämer U (2004) Cross-species microarray transcript profiling reveals high constitutive expression of metal homeostasis genes in shoots of the zinc hyperaccumulator Arabidopsis halleri. Plant J **3**: 251–268

Blanco F, Salinas P, Cecchini NM, Jordana X, Van Hummelen P, Alvarez ME, Holuigue L (2009) Early genomic responses to salicylic acid in Arabidopsis. Plant Mol Biol **70**: 79–102

Bus JS, Aust SD, Gibson JE (1976) Paraquat toxicity: proposed mechanism of action involving lipid peroxidation. Environ Health Perspect **16**: 139–146

Carr RJ, Bilton RF, Atkinson T (1985) Mechanism of biodegradation of paraquat by *Lipomyces starkeyi*. Appl Environ Microbiol **49**: 1290–1294

Chen I-C, Huang I-C, Liu M-J, Wang Z-G, Chung S-S, Hsieh H-L (2007) Glutathione *S*-transferase interacting with far-red insensitive 219 is involved in phytochrome A-mediated signaling in Arabidopsis. Plant Physiol **143**: 1189–1202

Chen J-H, Jiang H-W, Hsieh E-J, Chen H-Y, Chien C-T, Hsieh H-L, Lin T-P (2012) Drought and salt stress tolerance of an Arabidopsis glutathione *S*-transferase U17 knockout mutant are attributed to the combined effect of glutathione and abscisic acid. Plant Physiol **158**: 340–351

Chen W, Chao G, Singh KB (1996) The promoter of a H_2O_2-inducible, Arabidopsis glutathione S-transferase gene contains closely linked OBF- and OBP1-binding sites. Plant J 10: 955–966

Choi JH, Lou W, Vancura A (1998) A novel membrane-bound glutathione S-transferase functions in the stationary phase of the yeast Saccharomyces cerevisiae. J Biol Chem 273: 29915–29922

Choi YI, Noh EW, Kim HJ, Shim D (2013) Overexpression of poplar GSTU51 confers selective tolerance to both mercury and methyl viologen but not to CDNB or cadmium in transgenic poplars. Plant Biotechnol Rep 7: 175–184

Chronopoulou E, Ataya FS, Pouliou F, Perperopoulou F, Georgakis N, Nianiou-Obeidat I, Madesis P, Ioannou E, Labrou NE (2017a) Structure, evolution and functional roles of plant glutathione transferases. In MA Hossain, MG Mostofa, P Diaz-Vivancos, DJ Burritt, M Fujita, L-SP Tran, eds, Glutathione in Plant Growth, Development, and Stress Tolerance, Springer, Berlin, pp 195–213

Chronopoulou E, Georgakis N, Nianiou-Obeidat I, Madesis P, Perperopoulou F, Pouliou F, Vasilopoulou E, Ioannou E, Ataya FS, Labrou NE (2017b) Plant glutathione transferases in abiotic stress response and herbicide resistance. In MA Hossain, MG Mostofa, P Diaz-Vivancos, DJ Burritt, M Fujita, L-SP Tran, eds,Glutathione in Plant Growth, Development, and Stress Tolerance, Springer, Berlin, pp 215–233

Clough SJ, Bent AF (1998) Floral dip: a simplified method for Agrobacterium-mediated transformation of Arabidopsis thaliana. Plant J 16: 735–743

Cochemé HM, Murphy MP (2008) Complex I is the major site of mitochondrial superoxide production by paraquat. J Biol Chem 283: 1786–1798

Collinson EJ, Grant CM (2003) Role of yeast glutaredoxins as glutathione S-transferases. J Biol Chem 278: 22492–22497

Cummins I, Bryant DN, Edwards R (2009) Safener responsiveness and multiple herbicide resistance in the weed black-grass (Alopecurus myosuroides). Plant Biotechnol J 7: 807–820

Cummins I, Cole DJ, Edwards R (1999) A role for glutathione transferases functioning as glutathione peroxidases in resistance to multiple herbicides in black-grass. Plant J 18: 285–292

Cummins I, Cole DJ, Edwards R (1997) Purification of multiple glutathione transferases involved in herbicide detoxification from wheat (Triticum aestivum L.) treated with the safener fenchlorazole-ethyl. Pestic Biochem Physiol 59: 35–49

Cummins I, Dixon DP, Freitag-Pohl S, Skipsey M, Edwards R (2011) Multiple roles for plant glutathione transferases in xenobiotic detoxification. Drug Metab Rev 43: 266–280

Cummins I, Wortley DJ, Sabbadin F, He Z, Coxon CR, Straker HE, Sellars JD, Knight K, Edwards L, Hughes D, et al. (2013) Key role for a glutathione transferase in multiple-herbicide resistance in grass weeds. Proc Natl Acad Sci USA 110: 5812–5817

Daudi A, Cheng Z, O'Brien JA, Mammarella N, Khan S, Ausubel FM, Bolwell GP (2012) The apoplastic oxidative burst peroxidase in Arabidopsis is a major component of pattern-triggered immunity. Plant Cell 24: 275–287

Delaunay A, Pflieger D, Barrault MB, Vinh J, Toledano MB (2002) A thiol peroxidase is an H_2O_2 receptor and redox-transducer in gene activation. Cell 111: 471–481

DeRidder BP, Dixon DP, Beussman DJ, Edwards R, Goldsbrough PB (2002) Induction of glutathione S-transferases in Arabidopsis by herbicide safeners. Plant Physiol 130: 1497–1505

Dixon D, Cole DJ, Edwards R (1997) Characterisation of multiple glutathione transferases containing the GST I subunit with activities toward herbicide substrates in Maize (Zea mays). Pestic Sci 50: 72–82

Dixon DP, Edwards R (2010) Glutathione transferases. Arabidopsis Book. doi: 10.1199/tab.0131

Dixon DP, Edwards R (2018) Protein-ligand fishing in planta for biologically active natural products using glutathione transferases. Front Plant Sci 9: 1659

Dixon DP, Hawkins T, Hussey PJ, Edwards R (2009) Enzyme activities and subcellular localization of members of the Arabidopsis glutathione transferase superfamily. J Exp Bot 60: 1207–1218

Dixon DP, Lapthorn A, Madesis P, Mudd EA, Day A, Edwards R (2008) Binding and glutathione conjugation of porphyrinogens by plant glutathione transferases. J Biol Chem 283: 20268–20276

Dixon DP, Skipsey M, Edwards R (2010) Roles for glutathione transferases in plant secondary metabolism. Phytochemistry 71: 338–350

Du B, Zhao W, An Y, Li Y, Zhang X, Song L, Guo C (2019) Overexpression of an alfalfa glutathione S-transferase gene improved the saline-alkali tolerance of transgenic tobacco. Biol Open 8: bio043505

Edwards R, Dixon DP, Walbot V (2000) Plant glutathione S-transferases: enzymes with multiple functions in sickness and in health. Trends Plant Sci 5: 193–198

Eljebbawi A, Guerrero YDCR, Dunand C, Estevez JM (2021) Highlighting reactive oxygen species as multitaskers in root development. iScience 24: 101978

Fricker MD (2016) Quantitative redox imaging software. Antioxid Redox Signal 24: 752–762

Furusawa I, Tanaka K, Thanutong P, Mizuguchi A, Yazaki M, Asada K (1984) Paraquat resistant tobacco calluses with enhanced superoxide dismutase activity. Plant Cell Physiol 25: 1247–1254

Gietz RD, Woods RA (2002) Transformation of yeast by lithium acetate/single-stranded carrier DNA/polyethylene glycol method. Meth Enzymol 350: 87–96

Gomez C, Conejero G, Torregrosa L, Cheynier V, Terrier N, Ageorges A (2011) In vivo grapevine anthocyanin transport involves vesicle-mediated trafficking and the contribution of anthoMATE transporters and GST. Plant J 67: 960–970

Gong H, Jiao Y, Hu W, Pua E (2005) Expression of glutathione-S-transferase and its role in plant growth and development in vivo and shoot morphogenesis in vitro. Plant Mol Biol 57: 53–66

Gronwald JW, Plaisance KL (1998) Isolation and characterization of glutathione S-transferase isozymes from sorghum. Plant Physiol 117: 877–892

Gruhler A, Schulze WX, Matthiesen R, Mann M, Jensen ON (2005) Stable isotope labeling of Arabidopsis thaliana cells and quantitative proteomics by mass spectrometry. Mol Cell Proteomics 4: 1697–1709

Gullner G, Komives T, Király L, Schröder P (2018) Glutathione S-transferase enzymes in plant-pathogen interactions. Front Plant Sci 9: 1836

Gutscher M, Sobotta MC, Wabnitz GH, Ballikaya S, Meyer AJ, Samstag Y, Dick TP (2009) Proximity-based protein thiol oxidation by H_2O_2-scavenging peroxidases. J Biol Chem 284: 31532–31540

Herrera-Vásquez A, Fonseca A, Ugalde JM, Lamig L, Seguel A, Moyano TC, Gutiérrez RA, Salinas P, Vidal EA, Holuigue L (2021) TGA class II transcription factors are essential to restrict oxidative stress in response to UV-B stress in Arabidopsis. J Exp Bot 72: 1891–1905

Hooper CM, Tanz SK, Castleden IR, Vacher MA, Small ID, Millar AH (2014) SUBAcon: a consensus algorithm for unifying the subcellular localization data of the Arabidopsis proteome. Bioinformatics 30: 3356–3364

Ishiga Y, Ishiga T, Uppalapati SR, Mysore KS (2011) Arabidopsis seedling flood-inoculation technique: a rapid and reliable assay for studying plant-bacterial interactions. Plant Methods 7: 32

Ito J, Batth TS, Petzold CJ, Redding-Johanson AM, Mukhopadhyay A, Verboom R, Meyer EH, Millar AH, Heazlewood JL (2011) Analysis of the Arabidopsis cytosolic proteome highlights subcellular partitioning of central plant metabolism. J Proteome Res 10: 1571–1582

Jiang H-W, Liu M-J, Chen I-C, Huang C-H, Chao L-Y, Hsieh H-L (2010) A glutathione S-transferase regulated by light and

hormones participates in the modulation of Arabidopsis seedling development. Plant Physiol **154**: 1646–1658

Kao C-W, Bakshi M, Sherameti I, Dong S, Reichelt M, Oelmüller R, Yeh K-W (2016) A Chinese cabbage (*Brassica campetris* subsp. Chinensis) τ-type glutathione-S-transferase stimulates Arabidopsis development and primes against abiotic and biotic stress. Plant Mol Biol **92**: 643–659

Karimi M, Inzé D, Depicker A (2002) GATEWAY vectors for *Agrobacterium*-mediated plant transformation. Trends Plant Sci **7**: 193–195

Krajewski MP, Kanawati B, Fekete A, Kowalski N, Schmitt-Kopplin P, Grill E (2013) Analysis of Arabidopsis glutathione-transferases in yeast. Phytochemistry **91**: 198–207

Kumar S, Trivedi PK (2018) Glutathione S-transferases: role in combating abiotic stresses including arsenic detoxification in plants. Front Plant Sci **9**: 751

Labrou NE, Papageorgiou AC, Pavli O, Flemetakis E (2015) Plant GSTome: structure and functional role in xenome network and plant stress response. Curr Opin Biotechnol **32**: 186–194

Landi M (2017) Commentary to: "Improving the thiobarbituric acid-reactive-substances assay for estimating lipid peroxidation in plant tissues containing anthocyanin and other interfering compounds" by Hodges et al., Planta (1999) 207:604–611. Planta **245**: 1067

Laporte D, Olate E, Salinas P, Salazar M, Jordana X, Holuigue L (2012) Glutaredoxin GRXS13 plays a key role in protection against photooxidative stress in Arabidopsis. J Exp Bot **63**: 503–515

Liu Z-J, Zhang X-L, Bai J-G, Suo B-X, Xu P-L, Wang L (2009) Exogenous paraquat changes antioxidant enzyme activities and lipid peroxidation in drought-stressed cucumber leaves. Sci Hortic **121**: 138–143

Loeffler C, Berger S, Guy A, Durand T, Bringmann G, Dreyer M, von Rad U, Durner J, Mueller MJ (2005) B1-Phytoprostanes trigger plant defense and detoxification responses. Plant Physiol **137**: 328–340

Loyall L, Uchida K, Braun S, Furuya M, Frohnmeyer H (2000) Glutathione and a UV light-induced glutathione S-transferase are involved in signaling to chalcone synthase in cell cultures. Plant Cell **12**: 1939–1950

Mano J, Ohno C, Domae Y, Asada K (2001) Chloroplastic ascorbate peroxidase is the primary target of methylviologen-induced photooxidative stress in spinach leaves: its relevance to monodehydroascorbate radical detected with *in vivo* ESR. Biochim Biophys Acta **1504**: 275–287

Marrs KA (1996) The functions and regulation of glutathione S-transferases in plants. Annu Rev Plant Physiol Plant Mol Biol **47**: 127–158

Marty L, Siala W, Schwarzländer M, Fricker MD, Wirtz M, Sweetlove LJ, Meyer Y, Meyer AJ, Reichheld J-P, Hell R (2009) The NADPH-dependent thioredoxin system constitutes a functional backup for cytosolic glutathione reductase in Arabidopsis. Proc Natl Acad Sci USA **106**: 9109–9114

Mauch F, Dudler R (1993) Differential induction of distinct glutathione-S-transferases of wheat by xenobiotics and by pathogen attack. Plant Physiol **102**: 1193–1201

May MJ, Leaver CJ (1993) Oxidative stimulation of glutathione synthesis in *Arabidopsis thaliana* suspension cultures. Plant Physiol **103**: 621–627

Meyer AJ (2008) The integration of glutathione homeostasis and redox signaling. J Plant Physiol **165**: 1390–1403

Misra HP, Gorsky LD (1981) Paraquat and NADPH-dependent lipid peroxidation in lung microsomes. J Biol Chem **256**: 9994–9998

Moctezuma E, Leyva E, Monreal E, Villegas N, Infante D (1999) Photocatalytic degradation of the herbicide "Paraquat." Chemosphere **39**: 511–517.

Moons A (2003) *Osgstu3* and *osgtu4*, encoding tau class glutathione S-transferases, are heavy metal- and hypoxic stress-induced and differentially salt stress-responsive in rice roots. FEBS Lett **553**: 427–432

Mueller LA, Goodman CD, Silady RA, Walbot V (2000) AN9, a petunia glutathione S-transferase required for anthocyanin sequestration, is a flavonoid-binding protein. Plant Physiol **123**: 1561–1570

Mueller S, Hilbert B, Dueckershoff K, Roitsch T, Krischke M, Mueller MJ, Berger S (2008) General detoxification and stress responses are mediated by oxidized lipids through TGA transcription factors in Arabidopsis. Plant Cell **20**: 768–785

Murashige T, Skoog F (1962) A revised medium for rapid growth and bio assays with tobacco tissue cultures. Physiol Plant **15**: 473–497

Murgia I, Tarantino D, Vannini C, Bracale M, Carravieri S, Soave C (2004) *Arabidopsis thaliana* plants overexpressing thylakoidal ascorbate peroxidase show increased resistance to Paraquat-induced photooxidative stress and to nitric oxide-induced cell death. Plant J Cell Mol Biol **38**: 940–953

Navrot N, Collin V, Gualberto J, Gelhaye E, Hirasawa M, Rey P, Knaff DB, Issakidis E, Jacquot J-P, Rouhier N (2006) Plant glutathione peroxidases are functional peroxiredoxins distributed in several subcellular compartments and regulated during biotic and abiotic stresses. Plant Physiol **142**: 1364–1379

Nietzel T, Elsässer M, Ruberti C, Steinbeck J, Ugalde JM, Fuchs P, Wagner S, Ostermann L, Moseler A, Lemke P, et al. (2019) The fluorescent protein sensor roGFP2-Orp1 monitors *in vivo* H_2O_2 and thiol redox integration and elucidates intracellular H_2O_2 dynamics during elicitor-induced oxidative burst in Arabidopsis. New Phytol **221**: 1649–1664

Noctor G, Mhamdi A, Chaouch S, Han Y, Neukermans J, Marquez-Garcia B, Queval G, Foyer CH (2012) Glutathione in plants: an integrated overview. Plant Cell Environ **35**: 454–484

Perl A, Perl-Treves R, Galili S, Aviv D, Shalgi E, Malkin S, Galun E (1993) Enhanced oxidative-stress defense in transgenic potato expressing tomato Cu, Zn superoxide dismutases. Theor Appl Genet **85**: 568–576

Prade L, Huber R, Bieseler B (1998) Structures of herbicides in complex with their detoxifying enzyme glutathione S-transferase—explanations for the selectivity of the enzyme in plants. Structure **6**: 1445–1452

Ronquist F, Huelsenbeck JP (2003) MrBayes 3: Bayesian phylogenetic inference under mixed models. Bioinformatics **19**: 1572–1574

Rosenwasser S, Rot I, Meyer AJ, Feldman L, Jiang K, Friedman H (2010) A fluorometer-based method for monitoring oxidation of redox-sensitive GFP (roGFP) during development and extended dark stress. Physiol Plant **138**: 493–502

Roxas VP, Lodhi SA, Garrett DK, Mahan JR, Allen RD (2000) Stress tolerance in transgenic tobacco seedlings that overexpress glutathione S-transferase/glutathione peroxidase. Plant Cell Physiol **41**: 1229–1234

Roxas VP, Smith RK, Allen ER, Allen RD (1997) Overexpression of glutathione S-transferase/glutathione peroxidase enhances the growth of transgenic tobacco seedlings during stress. Nat Biotechnol **15**: 988–991

Sappl PG, Carroll AJ, Clifton R, Lister R, Whelan J, Harvey Millar A, Singh KB (2009) The Arabidopsis glutathione transferase gene family displays complex stress regulation and co-silencing multiple genes results in altered metabolic sensitivity to oxidative stress. Plant J **58**: 53–68

Sappl PG, Oñate-Sánchez L, Singh KB, Millar AH (2004) Proteomic analysis of glutathione S-transferases of *Arabidopsis thaliana* reveals differential salicylic acid-induced expression of the plant-specific Phi and Tau classes. Plant Mol Biol **54**: 205–219

Scarpeci TE, Zanor MI, Carrillo N, Mueller-Roeber B, Valle EM (2008) Generation of superoxide anion in chloroplasts of *Arabidopsis thaliana* during active photosynthesis: a focus on rapidly induced genes. Plant Mol Biol **66**: 361–378

Schindelin J, Arganda-Carreras I, Frise E, Kaynig V, Longair M, Pietzsch T, Preibisch S, Rueden C, Saalfeld S, Schmid B, et al.

(2012) Fiji: an open-source platform for biological-image analysis. Nat Methods **9**: 676–682

Schwarzländer M, Dick TP, Meyer AJ, Morgan B (2016) Dissecting redox biology using fluorescent protein sensors. Antioxid Redox Signal **24**: 680–712

Seguel A, Jelenska J, Herrera-Vásquez A, Marr SK, Joyce MB, Gagesch KR, Shakoor N, Jiang S-C, Fonseca A, Wildermuth MC, et al. (2018) PROHIBITIN3 forms complexes with ISOCHORISMATE SYNTHASE1 to regulate stress-induced salicylic acid biosynthesis in Arabidopsis. Plant Physiol **176**: 2515–2531

Shapiguzov A, Vainonen JP, Hunter K, Tossavainen H, Tiwari A, Järvi S, Hellman M, Aarabi F, Alseekh S, Wybouw B, et al. (2019) *Arabidopsis* RCD1 coordinates chloroplast and mitochondrial functions through interaction with ANAC transcription factors. eLife **8**: e43284

Sharma R, Sahoo A, Devendran R, Jain M (2014) Over-expression of a rice Tau class glutathione *S*-transferase gene improves tolerance to salinity and oxidative stresses in Arabidopsis. PLoS ONE **9**: e929000

Smirnoff N, Arnaud D (2019) Hydrogen peroxide metabolism and functions in plants. New Phytol **221**: 1197–1214

Sparkes IA, Runions J, Kearns A, Hawes C (2006) Rapid, transient expression of fluorescent fusion proteins in tobacco plants and generation of stably transformed plants. Nat Protoc **1**: 2019–2025

Stotz HU, Mueller S, Zoeller M, Mueller MJ, Berger S (2013) TGA transcription factors and jasmonate-independent COI1 signalling regulate specific plant responses to reactive oxylipins. J Exp Bot **64**: 963–975

Sylvestre-Gonon E, Law SR, Schwartz M, Robe K, Keech O, Didierjean C, Dubos C, Rouhier N, Hecker A (2019) Functional, structural and biochemical features of plant serinyl-glutathione transferases. Front Plant Sci **10**: 608

Tamura K, Hara-Nishimura I (2014) Functional insights of nucleocytoplasmic transport in plants. Front Plant Sci **5**: 118

Thom R, Cummins I, Dixon DP, Edwards R, Cole DJ, Lapthorn AJ (2002) Structure of a tau class glutathione *S*-transferase from wheat active in herbicide detoxification. Biochemistry **41**: 7008–7020

Timmerman KP (1989) Molecular characterization of corn glutathione *S*-transferase isozymes involved in herbicide detoxication. Physiol Plant **77**: 465–471

Tsukagoshi H, Busch W, Benfey PN (2010) Transcriptional regulation of ROS controls transition from proliferation to differentiation in the root. Cell **143**: 606–616

Ugalde JM, Fuchs P, Nietzel T, Cutolo EA, Homagk M, Vothknecht UC, Holuigue L, Schwarzländer M, Müller-Schüssele SJ, Meyer AJ (2021) Chloroplast-derived photo-oxidative stress causes changes in H_2O_2 and E_{GSH} in other subcellular compartments. Plant Physiol **186**: 125–141

Valenzuela-Chavira I, Contreras-Vergara CA, Arvizu-Flores AA, Serrano-Posada H, Lopez-Zavala AA, García-Orozco KD, Hernandez-Paredes J, Rudiño-Piñera E, Stojanoff V, Sotelo-Mundo RR, et al. (2017) Insights into ligand binding to a glutathione *S*-transferase from mango: structure, thermodynamics and kinetics. Biochimie **135**: 35–45

Veljovic-Jovanovic S, Noctor G, Foyer CH (2002) Are leaf hydrogen peroxide concentrations commonly overestimated? The potential influence of artefactual interference by tissue phenolics and ascorbate. Plant Physiol Biochem **40**: 501–507

Wagner U, Edwards R, Dixon DP, Mauch F (2002) Probing the diversity of the Arabidopsis glutathione *S*-transferase gene family. Plant Mol Biol **49**: 515–532

Waszczak C, Carmody M, Kangasjärvi J (2018) Reactive oxygen species in plant signaling. Annu Rev Plant Biol **69**: 209–236

Waterhouse AM, Procter JB, Martin DMA, Clamp M, Barton GJ (2009) Jalview Version 2—a multiple sequence alignment editor and analysis workbench. Bioinformatics **25**: 1189–1191

Wildermuth MC, Dewdney J, Wu G, Ausubel FM (2001) Isochorismate synthase is required to synthesize salicylic acid for plant defence. Nature **414**: 562–565

Xu J, Tian Y-S, Xing X-J, Peng R-H, Zhu B, Gao J-J, Yao Q-H (2016) Over-expression of At*GSTU19* provides tolerance to salt, drought and methyl viologen stresses in Arabidopsis. Physiol Plant **156**: 164–175

Yu T, Li YS, Chen XF, Hu J, Chang X, Zhu YG (2003) Transgenic tobacco plants overexpressing cotton glutathione *S*-transferase (GST) show enhanced resistance to methyl viologen. J Plant Physiol **160**: 1305–1311

Zhang Y, Tessaro MJ, Lassner M, Li X (2003) Knockout analysis of Arabidopsis transcription factors *TGA2*, *TGA5*, and *TGA6* reveals their redundant and essential roles in systemic acquired resistance. Plant Cell **15**: 2647–2653

Zhao F, Zhang H (2006) Salt and paraquat stress tolerance results from co-expression of the *Suaeda salsa* glutathione *S*-transferase and catalase in transgenic rice. Plant Cell Tissue Organ Cult **86**: 349–358